Supporting Information

Electronically Modified Cobalt Aminopyridine Complexes Reveal an Orthogonal Axis for Catalytic Optimization for CO_2 Reduction

Alon Chapovetsky,[†] Jeffrey J. Liu,[†] Matthew Welborn,[‡] John M. Luna,[†] Thomas Do,[†] Ralf Haiges,[†] Thomas F. Miller III,[*,‡] and Smaranda C. Marinescu[*,†]

[†]Department of Chemistry, University of Southern California, Los Angeles, California 90089, United States

[‡]Division of Chemistry and Chemical Engineering, California Institute of Technology, Pasadena, California 91125, United States

*Corresponding Authors: Smaranda C. Marinescu (smarines@usc.edu) and Thomas F. Miller III (tfm@caltech.edu)

Contents

General

All manipulations of air and moisture sensitive materials were conducted under a nitrogen atmosphere in a Vacuum Atmospheres drybox or on a dual manifold Schlenk line. The glassware was oven-dried prior to use. All solvents were degassed with nitrogen and passed through activated alumina columns and stored over 4Å Linde-type molecular sieves. Deuterated solvents were dried over 4Å Linde-type molecular sieves prior to use. Proton NMR spectra were acquired at room temperature using Varian (Mercury 400 2-Channel, VNMRS-500 2-Channel, VNMRS- 600 3-Channel, and 400-MR 2-Channel) spectrometers and referenced to the residual ^{1}H resonances of the deuterated solvent (^{1}H: $CDCl_3$, δ 7.26; C_6D_6, δ 7.16; CD_2Cl_2, δ 5.32; CD_3CN, δ 1.94) and are reported as parts per million relative to tetramethylsilane. Elemental analyses were performed using Thermo Scientific™ FLASH 2000 CHNS/O Analyzers. All the chemical reagents were purchased from commercial vendors and used without further purification.

Cyclic Voltammetry (CV)

Electrochemistry experiments were carried out using a Pine potentiostat. The experiments were performed in a single compartment electrochemical cell under nitrogen or CO_2 atmosphere using a 3 mm diameter glassy carbon electrode as the working electrode, a platinum wire as auxiliary electrode and a silver wire as the reference electrode. Ohmic drop was compensated using the positive feedback compensation implemented in the instrument. All reported potentials are referenced relative to ferrocene (Fc) with the $Fe^{3+/2+}$ couple at 0.0 V. Alternatively, in cases when the redox couple of ferrocene overlapped with other redox waves of interested, decamethylferrocene (Fc*) was as an internal standard with the $Fe^{*3+/2+}$ couple at –0.48 V. All electrochemical experiments were performed with 0.1 M tetrabutylammonium hexafluorophosphate as supporting electrolyte. The concentrations of the cobalt complexes **1–4** were generally at 0.5 mM and experiments with CO_2 were performed at gas saturation or varying amounts of CO_2 in dimethylformamide (DMF).

Controlled-potential electrolysis (CPE)

CPE measurements were conducted in a two-chambered H cell. The first chamber held the working and reference electrodes in 50 mL of 0.1 M tetrabutylammonium hexafluorophosphate and 1.3 M trifluoroethanol in DMF. The second chamber held the auxiliary electrode in 25 mL of 0.1 M tetrabutylammonium hexafluorophosphate in DMF. The two chambers were separated by a fine porosity glass frit. The reference electrode was placed in a separate compartment and connected by a Vycor tip. Glassy carbon plate electrodes (6 cm × 1 cm × 0.3 cm; Tokai Carbon USA) were used as the working and auxiliary electrodes. Using a gas-tight syringe, 10 mL of gas were withdrawn from the headspace of the H cell and injected into a gas chromatography instrument (Shimadzu GC-2010-Plus) equipped with a BID detector and a Restek ShinCarbon ST Micropacked column. Faradaic efficiencies were determined by diving the measured CO produced by the amount of CO expected based on the charge passed during the bulk electrolysis experiment. For each species the controlled-potential electrolysis measurements were performed at least twice, leading to similar behavior. The reported Faradaic efficiencies and mmol of CO produced are average values.

X-ray Diffraction Data Collection and Processing

The X-ray intensity data were collected on a Bruker APEX DUO 3-circle platform diffractometer with the χ-axis fixed at 50.74°, and using Mo K_α radiation (λ = 0.71073 Å) from a fine-focus tube monochromatized by a TRIUMPH curved-crystal monochromator.[1] The diffractometer was equipped with an APEX II CCD detector and an Oxford Cryosystems Cryostream 700 apparatus for low-temperature data collection adjusted to 173(2) K. The crystal was mounted in a Cryo-Loop using Paratone oil. A complete hemisphere of data was scanned on omega (0.5°) at a detector distance of 50 mm and a resolution of 512 x 512 pixels. The frames were integrated using the SAINT algorithm[2] to give the hkl files corrected for Lp/decay. Data were corrected for absorption effects using the multi-scan method (SADABS).[3] The structures were solved by intrinsic phasing and refined with the Bruker SHELXTL Software Package.[4–7]

Calculation of Binding Constant from Cyclic Voltammetry[8]

The CV's for complex **4** under N_2 and CO_2 are indicative of CO_2 binding to the metal center which can be approximated using the following equation

$$\Delta E = \left(\frac{RT}{nF}\right) ln\left(1 + [CO_2]K_Q\right) \qquad (6)$$

In Eq (6), ΔE corresponds to the change in potential (59 mV) for the $Co^{I/0}$ couple when the atmosphere is changed from N_2 to CO_2. R is the universal gas constant (8.314 J K^{-1} mol^{-1}), T is the temperature Kelvin (298.15 K), F is faraday's constant (96,485 C mol^{-1}), n is the number of electrons involve in the reduction from Co^I to Co^0 (1 electron), [CO_2] is the concentration of CO_2 in DMF (0.2 M) and K_Q is the binding constant between CO_2 and the cobalt catalyst.

Calculations of the Hammett Parameters for 1-4

The cumulative Hammett Parameters for **1-4** were calculated by the summation of the individual Hammett constants for each substituent. The literature[9] values used were:

$\sigma_{p,H} = 0$
$\sigma_{p,CF3} = 0.54$
$\sigma_{p,NMe2} = -0.83$

For complex **1**, 0×4 = **0**
For complex **2**, 0.54×4 = **2.16**
For complex **3**, $2 \times 0 + 2 \times (-0.83)$ = **−1.66**
For complex **4**, $2 \times 0.54 + 2 \times (-0.83)$ = **−0.58**

Crystallographic data

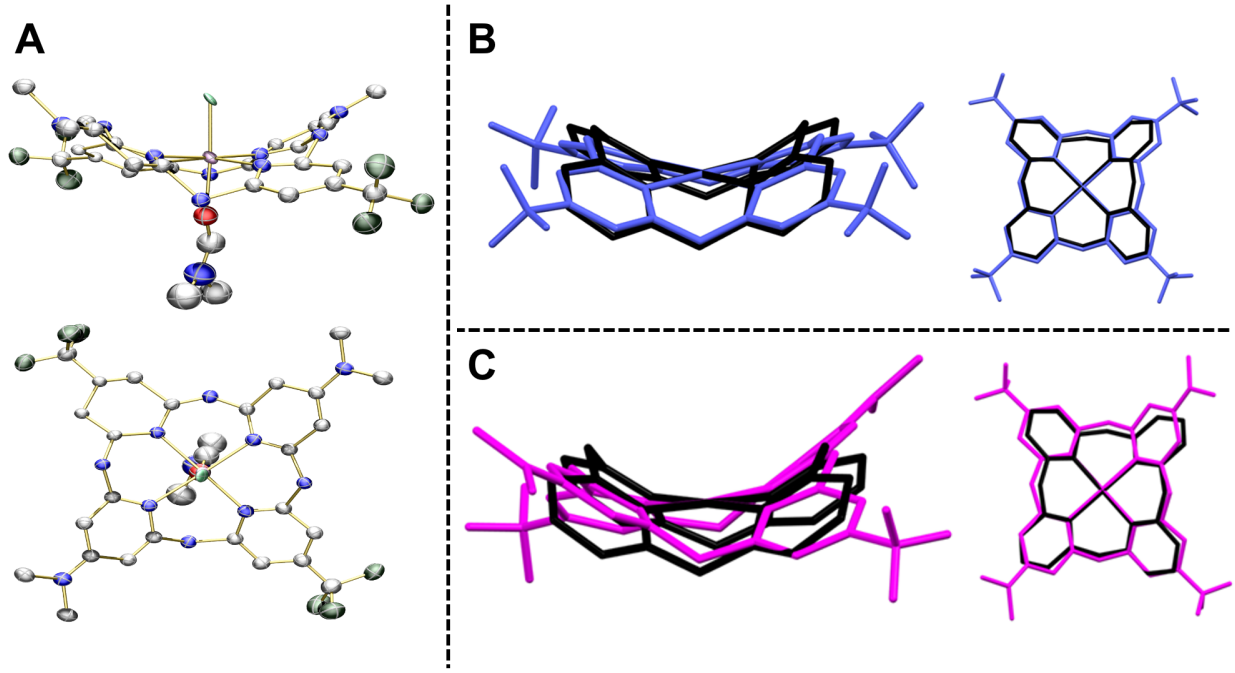

Figure S1. (**A**) Thermal ellipsoid drawing of complex **4** displayed at 50% probability level. Hydrogen atoms and BF_4^- counteranions are omitted for clarity. (**B**) Overlay of wireframe representations of complexes **2** (blue) and the unsubstituted cobalt aminopyridine **1** (black). (**C**) Overlay of wireframe representations of complexes **4** (blue) and the unsubstituted cobalt aminopyridine **1** (black).

Table S1. Sample and crystal data for 2.

Chemical formula	$C_{112}H_{72}B_8Co_4F_{80}N_{40}$	
Formula weight	3820.29 g/mol	
Temperature	100(2) K	
Wavelength	0.71073 Å	
Crystal size	0.207 × 0.210 × 0.390 mm	
Crystal habit	clear orange-red prism	
Crystal system	monoclinic	
Space group	$P_{1\ 21/c\ 1}$	
Unit cell dimensions	a = 19.663(4) Å	α = 90.00(3)°
	b = 10.366(2) Å	β = 115.34(3)°
	c = 19.730(4) Å	γ = 90.00(3)°
Volume	3634.6(15) Å^3	
Z	1	
Density (calculated)	1.745 g/cm^3	
Absorption coefficient	0.614 mm^{-1}	
F(000)	1892	
Diffractometer	Bruker APEX DUO	
Radiation source	fine-focus tube, MoKα	
Theta range for data collection	1.15 to 30.66°	
Index ranges	$-28 \le h \le 28$, $-14 \le k \le 14$, $-28 \le l \le 28$	
Reflections collected	87008	
Independent reflections	11058 [R(int) = 0.0356]	
Coverage of independent reflections	98.4%	
Absorption correction	multi-scan	
Max. and min. transmission	0.8830 and 0.7960	
Structure solution technique	direct methods	
Structure solution program	SHELXTL XT 2014/5 (Bruker AXS, 2014)	
Refinement method	Full-matrix least-squares on F^2	
Refinement program	SHELXTL XL 2014/7 (Bruker AXS, 2014)	
Function minimized	$\Sigma\, w(F_o^2 - F_c^2)^2$	
Data / restraints / parameters	11058 / 29 / 607	
Goodness-of-fit on F^2	1.027	
Δ/σ_{max}	0.002	
Final R indices	8892 data; I>2σ(I)	R_1 = 0.0485, wR_2 = 0.1221
	all data	R_1 = 0.0635, wR_2 = 0.1371
Weighting scheme	$w = 1/[\sigma^2(F_o^2)+(0.0618P)^2+5.1672P]$ where $P = (F_o^2+2F_c^2)/3$	
Largest diff. peak and hole	0.921 and –0.658 eÅ^{-3}	
R.M.S. deviation from mean	0.084 eÅ^{-3}	

Table S2. Sample and crystal data for 4–Cl.

Chemical formula	$C_{29}H_{27}BClCoF_{10}N_{11}O$	
Formula weight	840.80 g/mol	
Temperature	101(2) K	
Wavelength	1.54178 Å	
Crystal size	0.058 × 0.076 × 0.089 mm	
Crystal system	triclinic	
Space group	$P\bar{1}$	
Unit cell dimensions	a = 11.7413(11) Å	α = 85.400(8)°
	b = 13.0244(15) Å	β = 86.477(7)°
	c = 14.1477(15) Å	γ = 81.459(8)°
Volume	2129.9(4) Å^3	
Z	2	
Density (calculated)	1.311 g/cm^3	
Absorption coefficient	4.460 mm^{-1}	
F(000)	850	

Diffractometer	Bruker APEX DUO
Radiation source	IuS microsource (CuKα , λ = 1.54178 Å)
Theta range for data collection	3.14 to 59.20°
Index ranges	$-13 \le h \le 13$, $-14 \le k \le 14$, $-14 \le l \le 15$
Reflections collected	64274
Independent reflections	6042 [R(int) = 0.2056]
Coverage of independent reflections	97.9%
Absorption correction	multi-scan
Max. and min. transmission	0.7483 and 0.4221
Structure solution technique	direct methods
Structure solution program	SHELXTL XT 2014/4 (Bruker AXS, 2014)
Refinement method	Full-matrix least-squares on F^2
Refinement program	SHELXL-2018/3 (Sheldrick, 2018)
Function minimized	$\Sigma\, w(F_o^2 - F_c^2)^2$
Data / restraints / parameters	6042 / 1604 / 666
Goodness-of-fit on F^2	1.117
Final R indices	4209 data; I>2σ(I) R_1 = 0.1421, wR_2 = 0.3845
	all data R_1 = 0.1788, wR_2 = 0.4389
Weighting scheme	$w = 1/[\sigma^2(F_o^2)+(0.3500P)^2]$ where $P = (F_o^2+2F_c^2)/3$
Extinction coefficient	0.0340(40)
Largest diff. peak and hole	3.530 and –1.161 eÅ^{-3}
R.M.S. deviation from mean	0.214 eÅ^{-3}

Electrochemical Experiments and Analyses

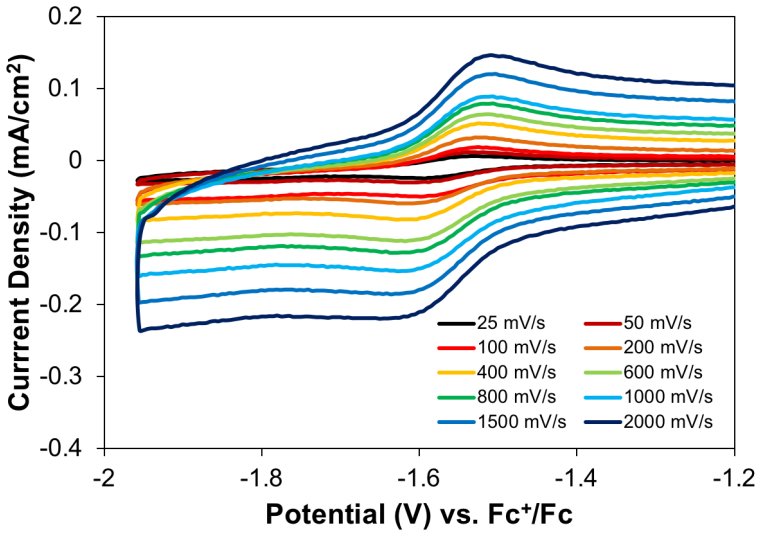

Figure S2. Cyclic voltammograms of complex **2** (0.5 mM) in a DMF solution containing 0.1 M [*n*Bu$_4$N][PF$_6$] under an atmosphere of N$_2$ displaying the reversible one-electron reduction with an $E_{1/2}$ of –1.56 V vs. Fc$^{+/0}$ and assigned to [Co(^{CF3}L)]$^{2+/+}$ couple. Scan rates vary from 0.025 to 2 V/s.

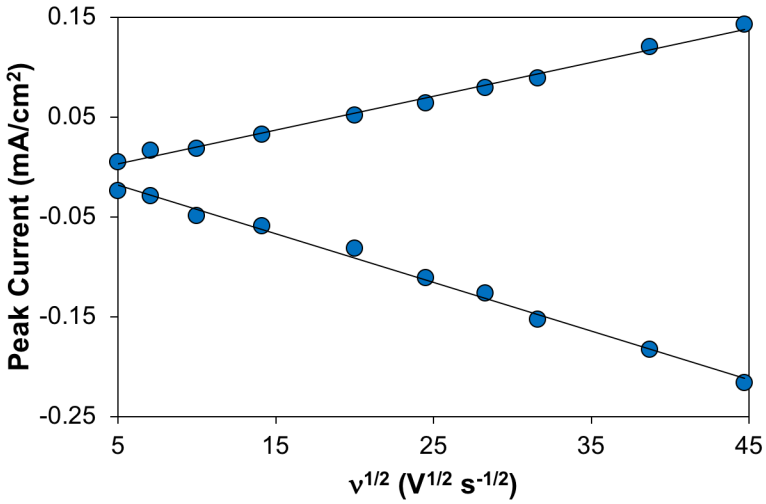

Figure S3. Plot showing the peak current, both cathodic and anodic, of complex **2** (0.5 mM in a DMF solution containing 0.1 M [*n*Bu$_4$N][PF$_6$] under an atmosphere of N$_2$) as a function of the scan rate. The cathodic and anodic peak currents increase linearly with the square root of the scan rate. This behavior is indicative of a freely-diffusing species, where the electrode reaction is controlled by mass transport.

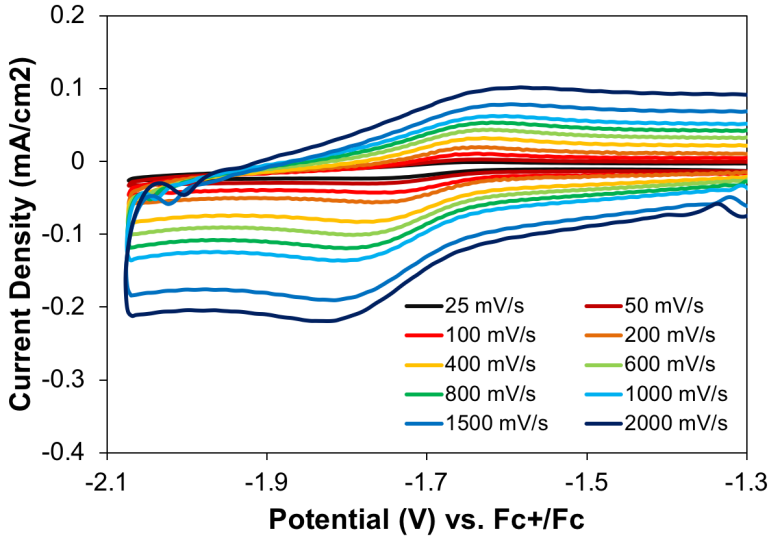

Figure S4. Cyclic voltammograms of complex **3** (0.5 mM) in a DMF solution containing 0.1 M [*n*Bu$_4$N][PF$_6$] under an atmosphere of N$_2$ displaying the reversible one-electron reduction with an $E_{1/2}$ of –1.75 V vs. Fc$^{+/0}$ and assigned to [Co(^{NMe2}L)]$^{2+/+}$ couple. Scan rates vary from 0.025 to 2 V/s.

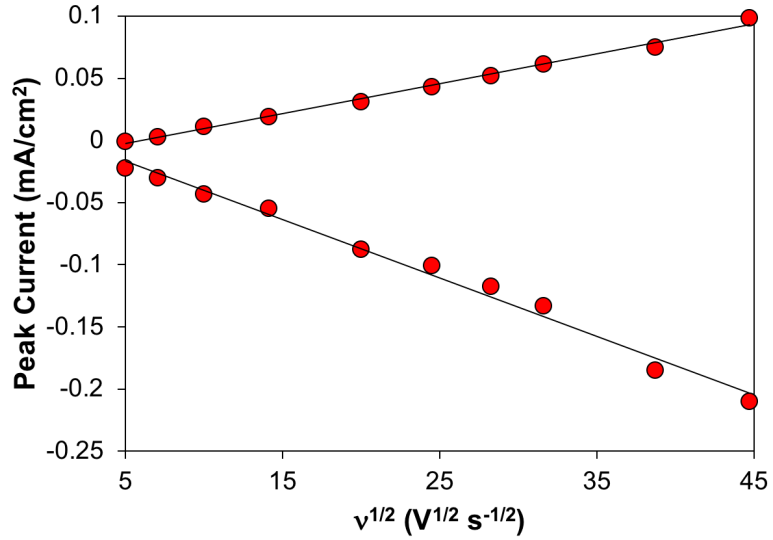

Figure S5. Plot showing the peak current, both cathodic and anodic, of complex **3** (0.5 mM in a DMF solution containing 0.1 M [*n*Bu$_4$N][PF$_6$] under an atmosphere of N$_2$) as a function of the scan rate. The cathodic and anodic peak currents increase linearly with the square root of the scan rate. This behavior is indicative of a freely-diffusing species, where the electrode reaction is controlled by mass transport.

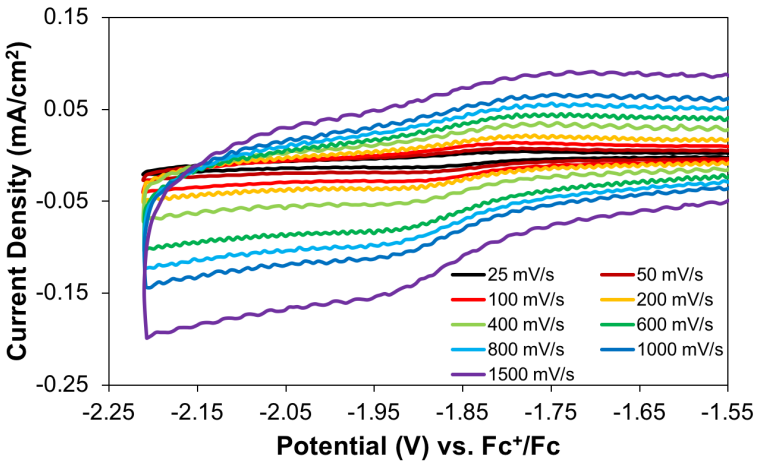

Figure S6. Cyclic voltammograms of complex **4** (0.5 mM) in a DMF solution containing 0.1 M [nBu$_4$N][PF$_6$] under an atmosphere of N$_2$ displaying the reversible one-electron reduction with an $E_{1/2}$ of –1.85 V vs. Fc$^{+/0}$ and assigned to [Co(^{Mix}L)]$^{2+/+}$ couple. Scan rates vary from 0.025 to 1.5 V/s.

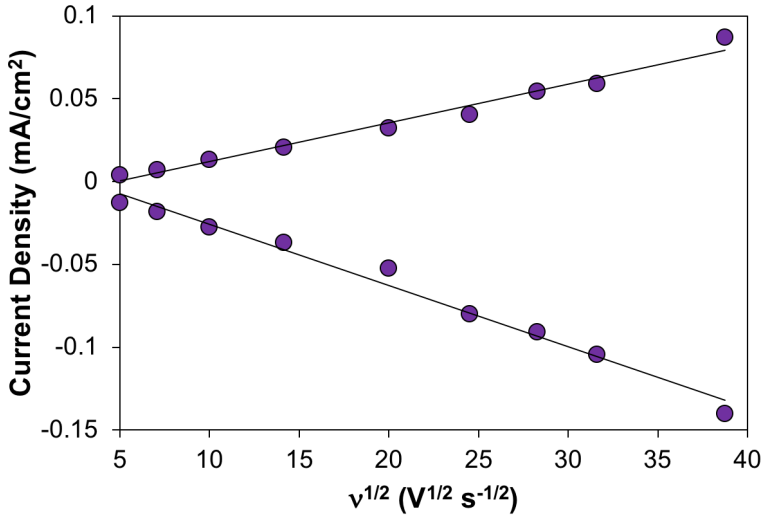

Figure S7. Plot showing the peak current, both cathodic and anodic, of complex **4** (0.5 mM in a DMF solution containing 0.1 M [nBu$_4$N][PF$_6$] under an atmosphere of N$_2$) as a function of the scan rate. The cathodic and anodic peak currents increase linearly with the square root of the scan rate. This behavior is indicative of a freely-diffusing species, where the electrode reaction is controlled by mass transport.

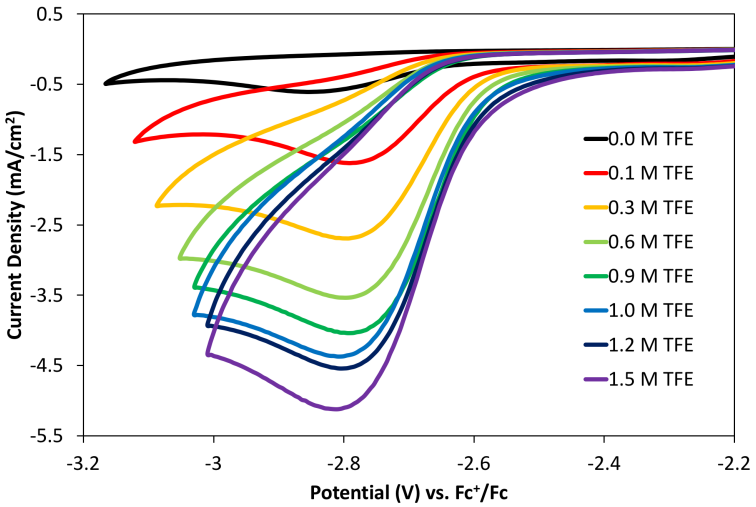

Figure S8. Cyclic voltammograms of complex **2** (0.5 mM) in a DMF solution containing 0.1 M [*n*Bu$_4$N][PF$_6$] under CO_2 atmosphere with varying amounts of TFE. The potential at which maximum current is observed is –2.72 V. Scans are performed at 100 mV/s.

Table S3. Catalytic current for the titration of complex **2** with TFE. i_p = 0.0177 mA/cm^2, extrapolated from the reversible $Co^{II/I}$ couple.

[TFE] (M)	i_{cat} (mA/cm^2)	i_{cat}/i_p
0.1	1.23	69.4
0.3	2.69	152.0
0.6	4.42	249.6
0.9	4.75	268.3
1.0	5.73	323.7
1.5	6.56	370.3

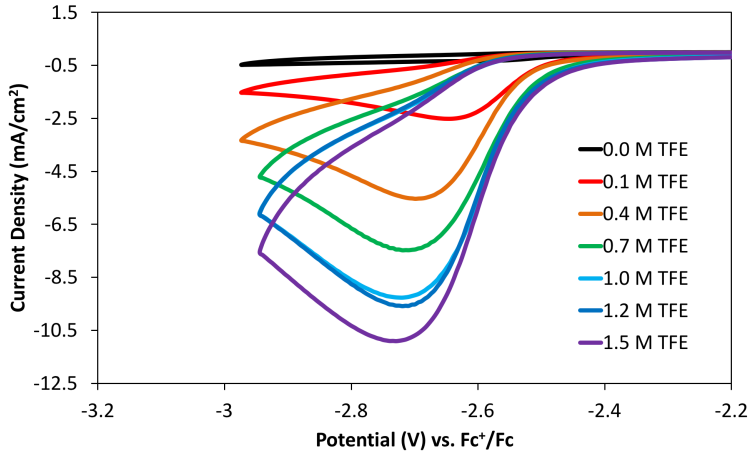

Figure S9. Cyclic voltammograms of complex **3** (0.5 mM) in a DMF solution containing 0.1 M [*n*Bu$_4$N][PF$_6$] under CO_2 atmosphere with varying amounts of TFE. The potential at which maximum current is observed is –2.73 V. Scans are performed at 100 mV/s.

Table S4. Catalytic current for the titration of complex **3** with TFE. i_p = 0.0140 mA/cm^2, extrapolated from the reversible $Co^{II/I}$ couple.

[TFE] (M)	i_{cat} (mA/cm^2)	i_{cat}/i_p
0.1	2.47	176.8
0.4	5.51	394.1
0.7	7.47	534.8
1.0	9.20	658.9
1.2	9.57	684.9
1.5	10.91	781.1

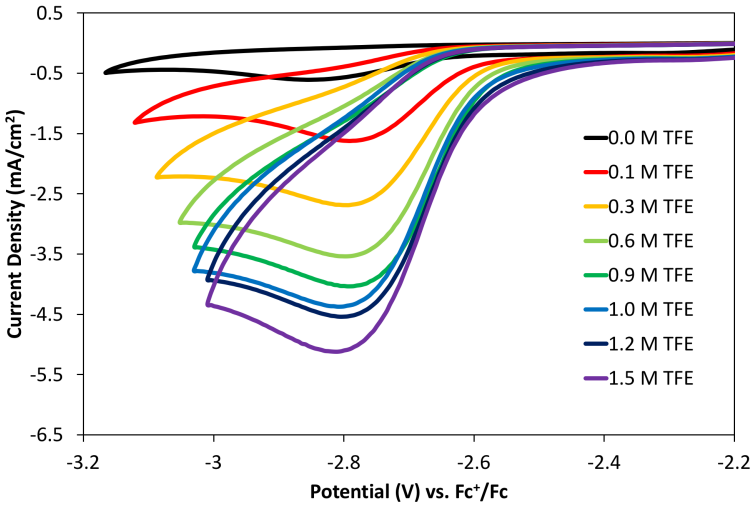

Figure S10. Cyclic voltammograms of complex **4** (0.5 mM) in a DMF solution containing 0.1 M [nBu$_4$N][PF$_6$] under CO_2 atmosphere with varying amounts of TFE. The potential at which maximum current is observed is –2.79 V. Scans are performed at 100 mV/s.

Table S5. Catalytic current for the titration of complex **4** with TFE. i_p = 0.0357 mA/cm^2, extrapolated from the reversible $Co^{II/I}$ couple.

[TFE] (M)	i_{cat} (mA/cm^2)	i_{cat}/i_p
0.1	1.62	45.4
0.3	2.69	75.4
0.6	3.53	98.9
0.9	4.00	112.1
1	4.369	122.4
1.2	4.546	127.4
1.5	5.123	143.5

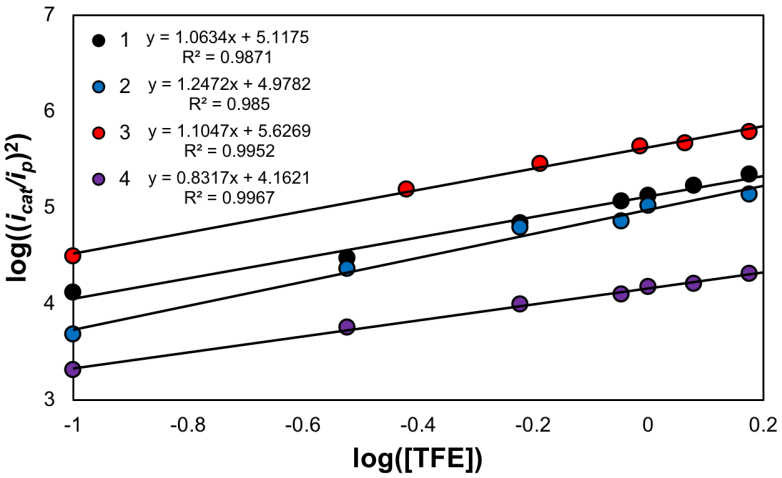

Figure S11. Plot of the log of $(i_{cat}/i_p)^2$ vs. log([TFE]). The slopes of the lines are all approximately equal to one indicating a reaction that is first order in protons.

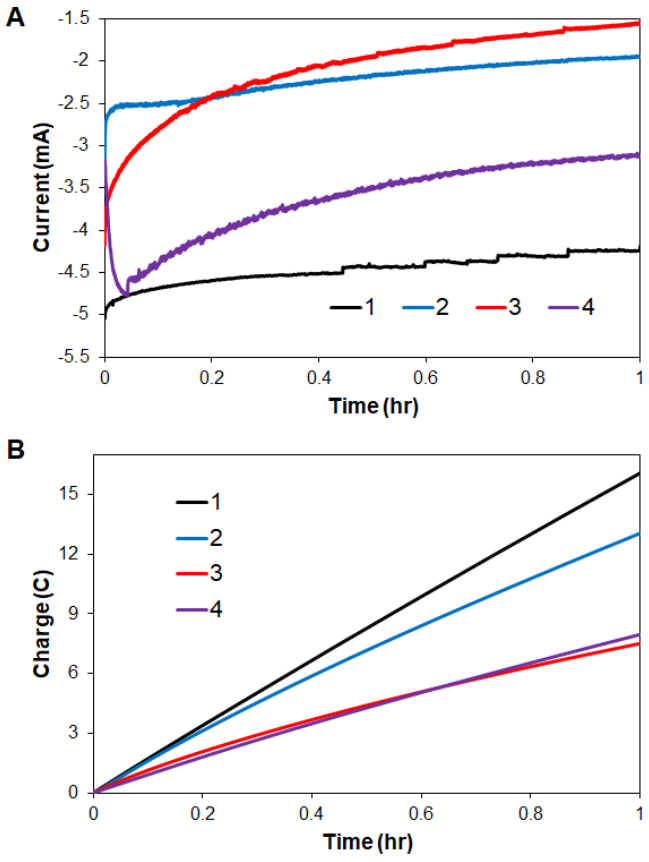

Figure S12. Overlay of the current (**A**) and charge (**B**) traces for the controlled potential electrolysis (CPE) experiments for complexes **1**–**4** measured at –2.75 V vs. $Fc^{+/0}$ over one hour. Electrochemical studies are performed in DMF solutions containing 0.1 M [nBu$_4$N][PF$_6$] under an atmosphere of CO_2 and in the presence of 2,2,2-trifluoroethanol (1.3 M) and catalyst (0.5 mM).

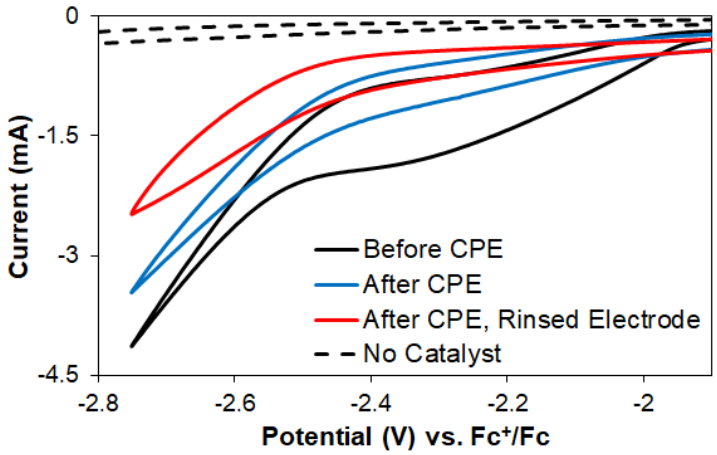

Figure S13. Cyclic voltammograms of complex **2** (0.5 mM) in a DMF solution containing [*n*Bu$_4$N][PF$_6$] (0.1 M), 2,2,2-trifluoroethanol (1.3 M), and CO_2 (1 atm) before (black) and after (blue) controlled potential electrolysis (CPE). After the controlled potential electrolysis, the working electrode was rinsed (3 × 10 mL DMF) and its electrochemistry was measured in a fresh DMF solution containing [*n*Bu$_4$N][PF$_6$] (0.1 M), 2,2,2-trifluoroethanol (1.3 M), and CO_2 (1 atm) – red trace. Scan rate = 100 mV/s.

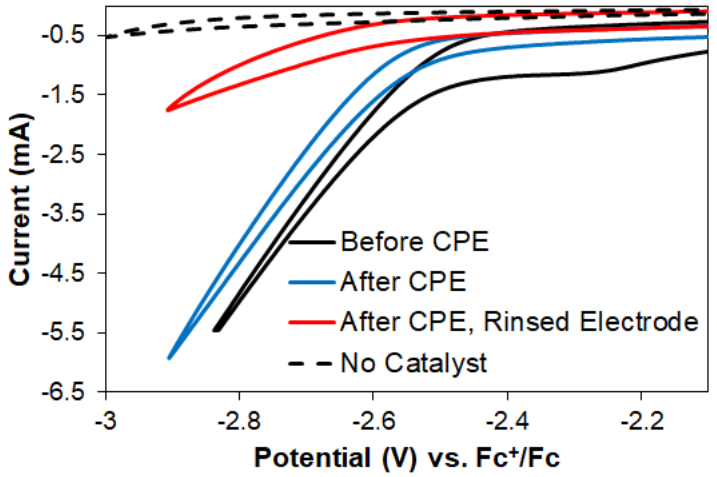

Figure S14. Cyclic voltammograms of complex **3** (0.5 mM) in a DMF solution containing [*n*Bu$_4$N][PF$_6$] (0.1 M), 2,2,2-trifluoroethanol (1.3 M), and CO_2 (1 atm) before (black) and after (blue) controlled potential electrolysis (CPE). After the controlled potential electrolysis, the working electrode was rinsed (3 × 10 mL DMF) and its electrochemistry was measured in a fresh DMF solution containing [*n*Bu$_4$N][PF$_6$] (0.1 M), 2,2,2-trifluoroethanol (1.3 M), and CO_2 (1 atm) – red trace. Scan rate = 100 mV/s.

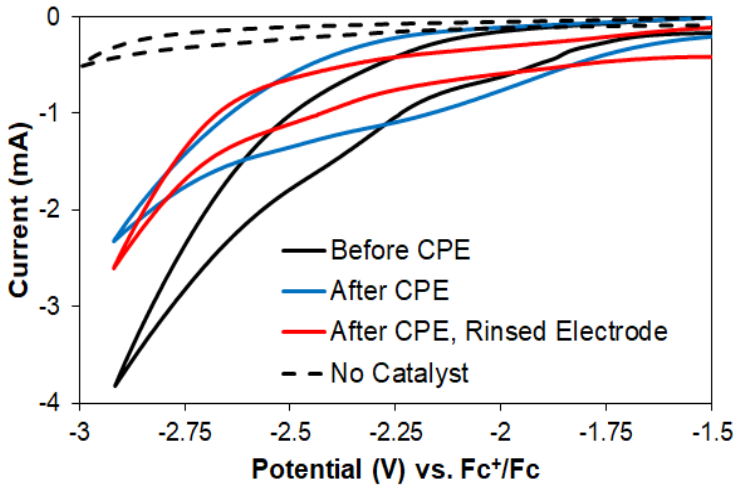

Figure S15. Cyclic voltammograms of complex **4** (0.5 mM) in a DMF solution containing [*n*Bu$_4$N][PF$_6$] (0.1 M), 2,2,2-trifluoroethanol (1.3 M), and CO_2 (1 atm) before (black) and after (blue) controlled potential electrolysis (CPE). After the controlled potential electrolysis, the working electrode was rinsed (3 × 10 mL DMF) and its electrochemistry was measured in a fresh DMF solution containing [*n*Bu$_4$N][PF$_6$] (0.1 M), 2,2,2-trifluoroethanol (1.3 M), and CO_2 (1 atm) – red trace. Scan rate = 100 mV/s.

Hammett Analysis

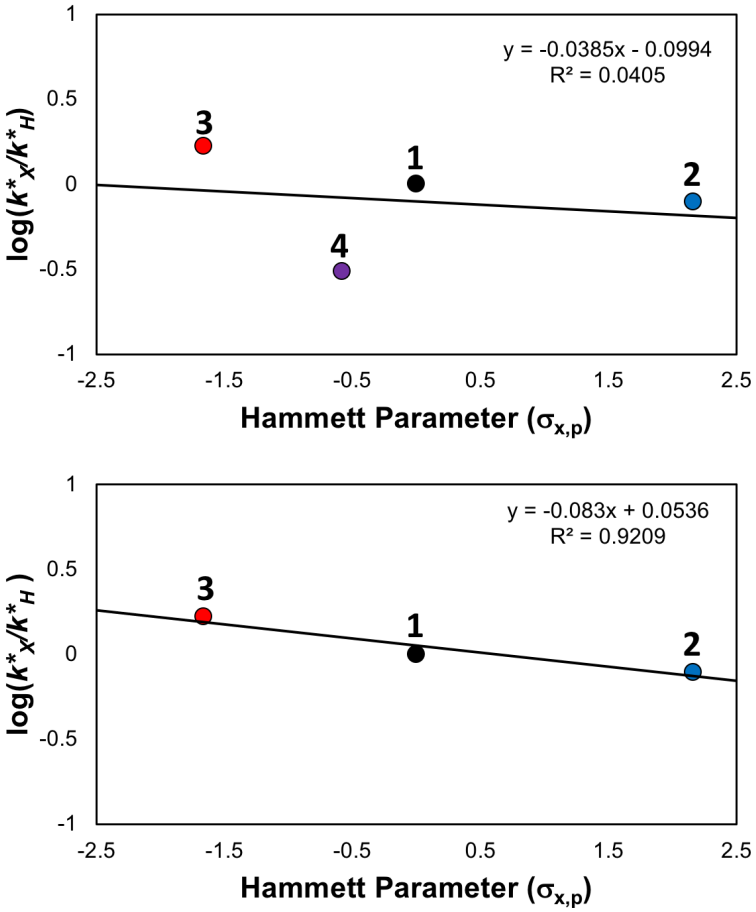

Figure S16. Hammett plot showing a linear free energy correlation between log of k^*_X/k^*_H ($k^* = (i_{cat}/i_p)^2$) and macrocycle substitution. Catalytic currents were measured in the presence of 1.5 M TFE under an atmosphere of CO_2. A negative slope indicates that the rate-determining step involves a buildup of positive charge or a decrease in negative charge, consistent with a protonation. While a weak correlation is observed when including the entire series ($R^2 = 0.0405$), removing complex **4**, which exhibits significant deposition, results in a strong correlation ($R^2 = 0.9209$) and a corresponding ρ value of –0.083. The Hammett parameters for each macrocycle were calculated by summing the individual Hammett constants for each pyridyl group (see page S3).

Density Functional Theory Calculation Details

Density Functional Theory (DFT) calculations are performed using the Q-Chem 5.0 software package.[10] The B3LYP functional is used for all calculations.[11–14] Calculations are done using the relatively-fine Lebedev exchange correlation grid with 75 radial and 302 points.[15] The 6-31+g* basis set is used for all calculations.[16] Diffuse functions are included to properly treat the strong anionic character of the bound CO_2 .

Dimethylformamide solvation energies are computed using the SMD implicit solvent model.[17] Solvent calculations are done, as recommended, at the gas phase optimized geometries. The SM12 model is also tested and yields similar results, but the CM5 charge component of the model does not converge for all geometries.

Geometry optimizations are started from initial guesses corresponding to the structures of complex **1**, and the resulting DFT minima do not deviate qualitatively from these initial guesses. All geometric minima are fully optimized to the default thresholds of the Q-Chem 5.0 software package. Protonation free energies are computed as described in a previous report of closely related cobalt macrocyclic derivatives.[18]

Schemes for ^{CF3}L, ^{NMe2}L, and ^{Mix}L Synthesis

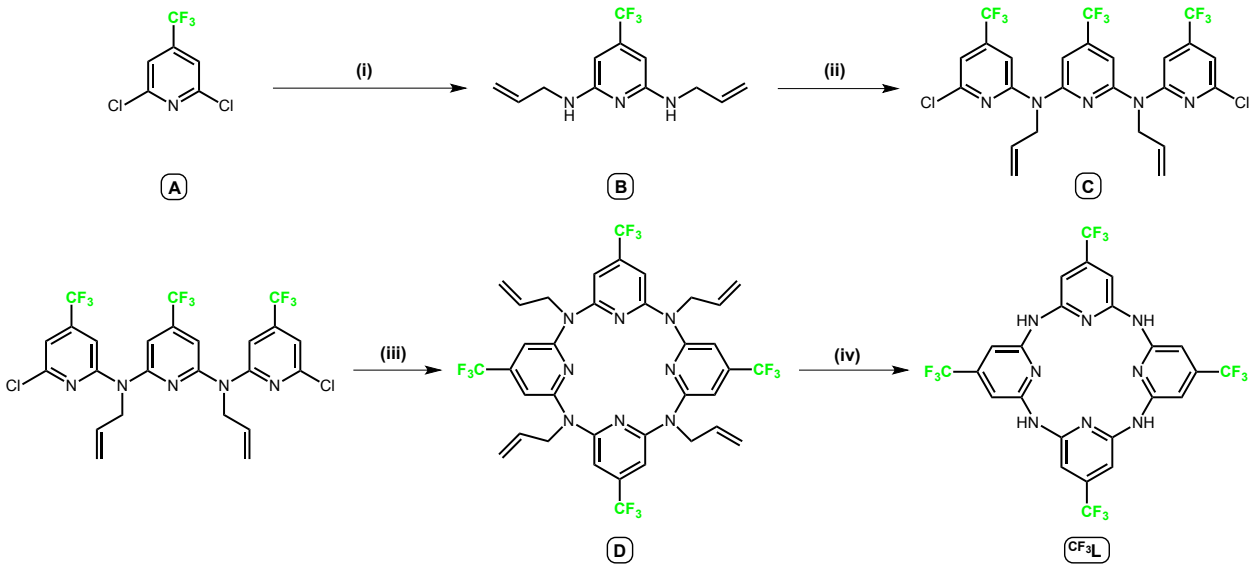

Figure S17. Synthetic scheme for the preparation of ^{CF3}**L**. (i) Allylamine, CuBr, L-Proline, K_2CO_3, 10:1 DMSO:H_2O, 135 °C, 72 h, 50% yield; (ii) **A**, NaH, THF, 80 °C, 2 h, 80% yield; (iii) **B**, **C**, $Pd_2(dba)_3$, dppf, NaO*t*Bu, toluene, 110 °C, 1 h, 20% yield; (iv) $Pd_2(dba)_3$, dppf, KO*t*Bu, toluene, 110 °C, 12 h, 70% yield, where dba = dibenzylacetone, and dppf = 1,1'-Bis(diphenylphosphino)ferrocene.

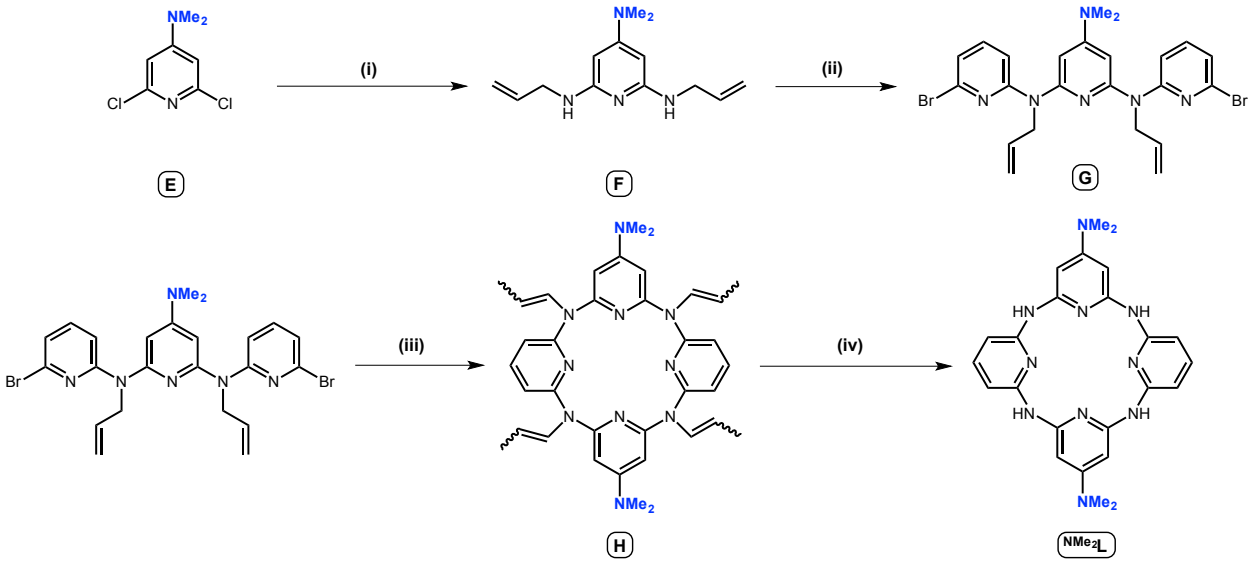

Figure S18. Synthetic scheme for the preparation of ^{NMe2}**L**. (i) Allylamine, $Pd_2(dba)_3$, dppp, NaO*t*Bu, toluene, 110 °C, 12 h, 30% yield; (ii) NaH, THF, 80 °C, 2,6-Dibromopyridine, 2 h, 65% yield; (iii) **F**, **G**, $Pd_2(dba)_3$, dppp, NaO*t*Bu, toluene, 110 °C, 1 h; (iv) HCl, 10:1 DMSO:H_2O, 60 °C, 1 h, 35% yield, where dba = dibenzylacetone, and dppp = 1,3-Bis(diphenylphosphino)propane.

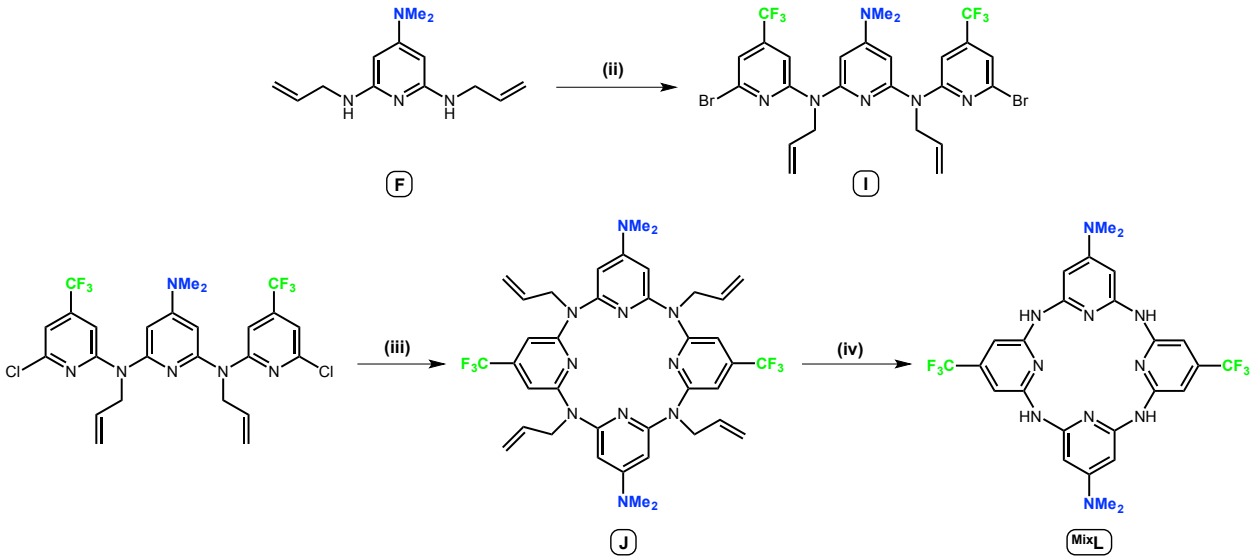

Figure S19. Synthetic scheme for the preparation of ^{Mix}**L**. (i) Allylamine, $Pd_2(dba)_3$, dppp, NaO*t*Bu, toluene, 110 °C, 12 h, 30% yield; (ii) **A**, NaH, THF, 80 ºC, 2 h, 70% yield; (iii), **I**, **F**, $Pd_2(dba)_3$, dppp, NaO*t*Bu, toluene, 110 °C, 1 h, 25% yield; (iv) $Pd_2(dba)_3$, dppf, KO*t*Bu, toluene, 110 °C, 12 h, 85% yield, where dba = dibenzylacetone, dppp = 1,3-Bis(diphenylphosphino)propane, and dppf = 1,1'-Bis(diphenylphosphino)ferrocene.

Synthetic Procedures

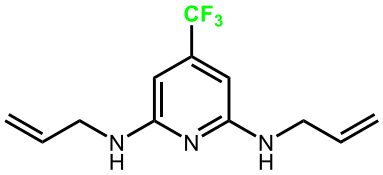

B

2,6-(bis)allylamino-4-(trifluromethyl)pyridine (B), 2,6-dichloro-4-(trifluromethyl)pyridine (5 g, 23.1 mmol), copper iodide (440.8 mg, 2.31 mmol), L-proline (532 mg, 4.62 mmol), and potassium carbonate (9.60 g, 69.4 mmol) were added to a nitrogen filled thick walled bomb flask. Degassed DMSO (60 mL), water (6 mL), and allylamine (17.36 mL, 231.0 mmol) were added to the above solids, and the flask was sealed under nitrogen and heated at 120 °C for 3 days. Upon cooling to room temperature, the red solution was filtered through Celite, and extracted with ethyl acetate (100 mL) and water (200 mL). The organic layer was separated and the aqueous layer was extracted with ethyl acetate (2 × 100 mL). The combined organic fractions were washed with water (10 × 100 mL) and dried with Na_2SO_4. Removal of solvent afforded the crude product as a black oil. The oil was chromatographed on a silica gel column using a 3:1 mixture of dichloromethane:hexanes as the mobile phase. After the removal of solvent, a white solid was obtained (51% yield). ^{1}H NMR (500 MHz, $CDCl_3$) δ 5.93 (m, 2H, *H*C=CH_2), 5.88 (s, 2H, *m*-NC_5H_2), 5.27-5.16 (dd, 4H, HC=C*H*$_2$), 4.56 (s, 2H, N*H*), 3.7 (d, 4H, *H*$_2$C-CH). ^{13}C{^{1}H} NMR (126 MHz, $CDCl_3$) δ 158.36, 134.92, 116.07, 90.77, 44.54. ^{19}F{^{1}H} NMR (470 MHz, $CDCl_3$) δ –65.46.

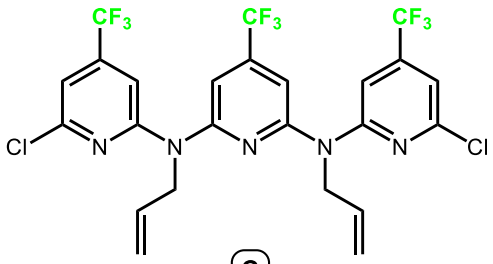

C

N2,N6-Bis(6-chloro-4-(trifluromethyl)pyridin-2-yl)-N2,N6-diallyl-4-(trifluromethyl)pyridine-2,6-diamine (C), NaH (60 wt% in paraffin liquid, 0.988 g, 24.7 mol) and 2,6-(bis)allylamino-4-(trifluromethyl)pyridine (1.06 g, 4.12 mmol) were added to a stir bar equipped, oven dried 100 mL 3-neck flask under nitrogen protection. THF (30 mL) was slowly added to generate an amber suspension. The mixture was then refluxed at 80 °C for one hour and then taken off the heat and allowed to cool. 2,6-dichloro-4-(trifluormethyl)pyridine (2.66 g, 12.3 mmol) was added to the mixture and the solution was brought back to reflux for 1.5 hours. The solution was allowed to cool to room temperature and slowly quenched with cold water. The solvent was removed under vacuum and the residue was dissolved in dichloromethane (50 mL). The organic layer was washed with water (3 × 100 mL), dried with Na_2SO_4 and concentrated under vacuum to give a brown oil. The oil was chromatographed on a silica gel column using a 2:1 mixture of dichloromethane:hexanes as the mobile phase. The product was the second to elute. After removal of solvent the product was isolated as an orange solid (81% yield). ^{1}H NMR (500 MHz, $CDCl_3$): δ 7.32 (s, 2H, central *m*-NC_5H_2), 7.13 (s, 2H, outer *m*-NC_5H_2), 7.10 (s, 2H, outer m-NC_5H_2), 5.92 (m, 2H *H*C=CH_2), 5.17 (dd, 4H, HC=C*H*$_2$), 4.79 (m, 4H, *H*$_2$C-CH). ^{13}C{^{1}H} NMR (126 MHz, $CDCl_3$): δ 156.22, 154.86, 132.64, 117.12, 112.90, 108.75, 104.29, 50.8. ^{19}F{^{1}H} NMR (470 MHz, $CDCl_3$) δ –65.02, –65.26.

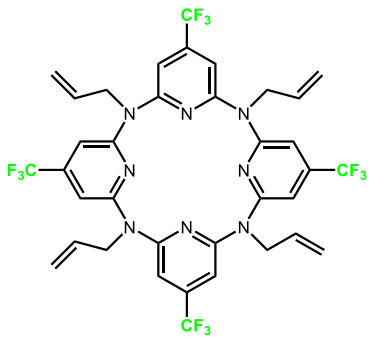

D

(NAllyl)$_4$-BridgedCalix[4]-4-(trifluromethyl)pyridine (Py$_4$(CF$_3$)$_4$(NAllyl)$_4$) (D), $Pd_2(dba)_3$ (55 mg, 0.06 mmol), 1,1'-Bis(diphenylphosphino)ferrocene (62.1 mg 0.11 mmol), and sodium *tert*-butoxide (111 mg 1.15 mmol) were added to a stir bar equipped, oven dried 100 mL 3-neck flask under nitrogen atmosphere. Dry toluene (100 mL) was syringed into the flask and the resultant red mixture was heated to 60 °C, when **B** (112.2 mg, 0.43 mmol), and **C** (226.3 mg, 0.37 mmol), were added to the suspension, causing a color change from red to orange. The reaction mixture was then

further heated to 110 °C and refluxed for 2.5 hours. After cooling to room temperature, the solution was filtered through Celite, reduced under pressure, and re-dissolved in dichloromethane (50 mL). The solution was washed with water (5 × 100 mL) and the aqueous layer was re-extracted with dichloromethane (2 × 50 mL). The combined organic layers were dried with Na_2SO_4 and eluted through a silica containing fritted glass funnel. The resultant organic fraction was reduced under pressure to give a yellow oil. The residue was chromatographed on a silica gel column using a 3:1 dichloromethane:hexane mobile phase. The desired product was the second compound to elute, and reduction of solvent under reduced pressure yielded a brown solid (20% yield). ^{1}H NMR (500 MHz, $CDCl_3$): δ 6.62 (s, 8H, m, 2H, *m*-NC_5H_2), 5.84 (m, 4H, *H*C=CH_2), 5.26-5.16 (dd, 8H, HC=C*H*$_2$), 4.38-4.20 (dd, 8H, *H*$_2$C-CH). ^{13}C{^{1}H} NMR (126 MHz, $CDCl_3$): δ 158.3, 133.05, 116.92, 105.34, 52.51. ^{19}F{^{1}H} NMR (470 MHz, $CDCl_3$): δ –64.88.

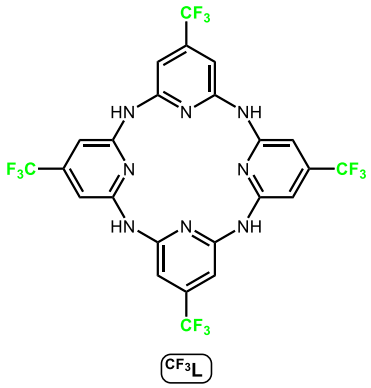

(NH)$_4$-BridgedCalix[4]-4-(trifluromethyl)pyridine (Py$_4$(CF$_3$)$_4$NH$_4$) (^{CF3}L), $Pd_2(dba)_3$ (2 mg, 2.1 mmol), 1,1'-Bis(diphenylphosphino)ferrocene (24 mg 4.3 mmol), and potassium *tert*-butoxide (37.4 mg, 0.33 mmol) were added to a stir bar equipped, oven dried 100 mL 3-neck flask under nitrogen atmosphere. Dry toluene (30 mL) was syringed into the flask and the resultant red mixture was heated. Upon reaching approximately 60 °C, **D** (45.0 mg, 0.056 mmol), was added to the suspension, causing a darkening in color. The reaction mixture was then heated to 110 °C and refluxed for 12 hours. After cooling to room temperature, the solvent was removed under reduced pressure and redissolved in dichloromethane (20 mL). The solution was washed with water (3 × 30 mL). The organic layers were dried with Na_2SO_4 and eluted through a 2.5 cm × 1 cm silica containing fritted glass funnel. The resultant organic fraction was reduced under pressure to give brown oil. The oil was dissolved in a 10:1 acetone:water mixture (10 mL) and excess concentrated hydrochloric acid was added. The resultant orange mixture was heated to reflux for an hour. The

acetone was removed under reduced pressure and $Na_2CO_{3(aq)}$ was added until the solution reached a pH of 10. The solution was filtered and the filtrate was washed with benzene. The filtrate was isolated and dried under vacuum to give **D** as an off-white solid (70% yield). ^{1}H NMR (500 MHz, acetone-d_6): δ 6.74 (s, 8H, *m*-NC_5H_2), 8.64 (s, 4H, N*H*). $^{13}C\{^1H\}$ NMR (126 MHz, $CDCl_3$): δ 158.31, 156.28, 150.01, 133.54, 118.31, 115.05, 109.35, 105.03, 50.11. $^{19}F\{^1H\}$ NMR (470 MHz, $CDCl_3$): δ –65.74.

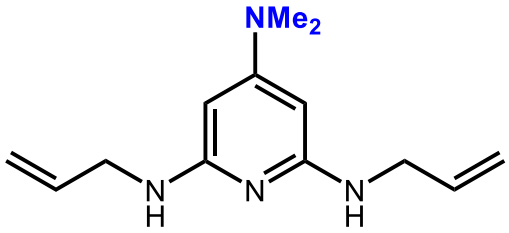

F

2,6-(bis)allylamino-4-(dimethylamine)pyridine (F), 2,6-dichloro-4-(dimethylamine)pyridine (**E**) (813.2 mg, 4.28 mmol), $Pd_2(dba)_3$ (177 mg, 0.19 mmol), 1,1'-Bis(diphenylphosphino)ferrocene (193.5 mg, 0.35 mmol), and sodium *tert*-butoxide (1.73 g, 18.0 mmol) were added to an oven dried, stir bar equipped, nitrogen filled thick walled bomb flask. Degassed toluene (250 mL) was added to the solution, along with allylamine (17.36 mL, 23.1 mmol). The flask was then sealed under nitrogen and heated at 110 °C overnight. **NOTE: This molecule is air sensitive. Work up must be performed as rapidly as possible.** Upon cooling to room temperature, the red solution was filtered through Celite, and the solvent was removed under reduced pressure. The obtained red residue was suspended in hexanes (80 mL) and sonicated for 25 minutes. The solution was filtered to remove the insoluble impurities. The solids were further washed with hexanes (2 × 80 mL) and filtered again. The hexane fractions were combined. Removal of the solvent gave rise to the product as an orange oil. The oil was immediately brought into an inert atmosphere glove box, extracted into pentane (25 mL) and mixed with crushed activated molecular sieves (~10 sieve spheres). The solution was stirred for 35 minutes before being filtered. The solvent was removed under reduced pressure to give the product as an amber oil in 30% yield. **NOTE: The oil MUST be stored under inert atmosphere.** ^{1}H NMR (500 MHz, $CDCl_3$): δ 5.93 (m, 2H, *H*C=CH_2), 5.27-5.16 (dd, 4H, HC=C*H*$_2$), 5.12 (s, 2H, *m*-NC_5H_2), 3.83 (m,

4H, H_2C-CH), 2.92 (s, 6H, N(CH_3)$_2$) $^{13}C\{^1H\}$ NMR (126 MHz, $CDCl_3$): δ 158.97, 158.15, 135.95, 115.53, 7.48, 45.24, 39.48.

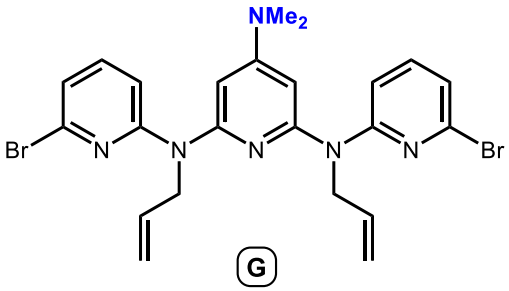

N2,N6-diallyl-N2,N6-bis(6-bro-4-(pyridin-2-yl)-N4,N4-dimethylpyridine-2,4,6-triamine (G), NaH (60 wt% in paraffin liquid, 600 mg, 15.0 mmol) and **E** (600 mg, 3.14 mmol) were added to a stir bar equipped, oven dried 100 mL 3-neck flask under nitrogen atmosphere. THF (30 mL) was slowly added to generate an amber suspension. The mixture was then refluxed at 80 °C for one hour and was then taken off heat and allowed to cool. 2,6-dibromopyridine (1.83 g, 7.73 mmol) was added to the mixture and the solution was brought back to reflux for 1 hour. The solution was cooled to room temperature and slowly quenched with cold water. The solvent was removed under vacuum and the residue was dissolved in dichloromethane (50 mL). The organic layer was washed with water (3 × 100 mL), dried with Na_2SO_4 and concentrated under vacuum to give a brown oil. The oil was chromotographed on a silica gel column with a 2:1 mixture of hexanes: dichloromethane as the mobile phase and then washed with diethyl ether to isolate the product as a yellow oil (73% yield). ^1H NMR (500 MHz, $CDCl_3$) δ 7.25 (t, 2H, *p*-pyridine), 7.03 (d, 2H, *m*-pyridine bromine adjacent), 6.89 (d, 2H, *m*-pyridine nitrogen adjacent), 6.30 (s, NMe_2-pyridine), 5.99 (m, 2H, HC=CH_2), 5.22-5.12 (dd, 4H, HC=CH_2), 4.72 (s, 4H, H_2C-CH). $^{13}C\{^1H\}$ NMR (126 MHz, $CDCl_3$): δ 157.52, 157.20, 155.81, 139.35, 138.58, 134.80, 118.39, 116.17, 111.35, 95.04, 50.76, 39.56.

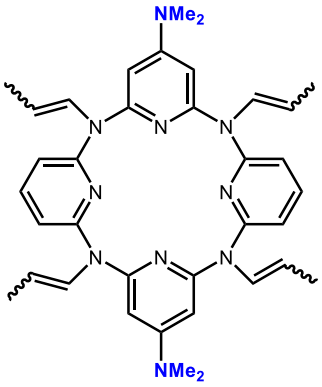

H

N^1_4,N^1_4,N^5_4,N^5_4-tetramethyl-2,4,6,8-tetra(prop-1-en-1-yl)-2,4,6,8-tetraaza-1,3,5(2,6)-tripyridina-7(1,3)-benzenacyclooctaphane-14,54-diamine (H). $Pd_2(dba)_3$ (35 mg, 0.038 mmol), 1,3-Bis(diphenylphosphino)propane (31.7 mg, 0.08 mmol), and sodium *tert*-butoxide (80 mg, 0.83 mmol) were added to a stir bar equipped, oven dried 250 mL 3-neck flask under nitrogen atmosphere. Dry toluene (70 mL) was syringed into the flask and the resultant red mixture was heated to 60 °C, when **G** (151.0 mg, 0.27 mmol) and **F** (59.4 mg, 0.26 mmol) were added to the suspension, causing a darkening in color. The reaction mixture was then further heated to 110 °C and refluxed for twelve hours. After cooling to room temperature, the solvent was removed under reduced pressure and redissolved in diethyl ether. The red solution was filtered through Celite and was used without further purification. Diagnostic proton NMR peaks can be found at 5.85 (singlet) and 6.45 (doublet).

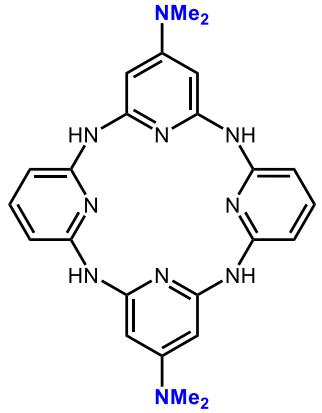

NMe_2L

$(NH)_4$-BridgedCalix[4]-pyridine-$(Py(NMe_2)_2(Py)_2)$ (^{NMe2}L). **H** was dissolved in a 10:1 acetone:water (11 mL) mixture and concentrated HCl was added (5 mL). The solution was refluxed for one hour, after which the volatiles were removed under reduced pressure. $Na_2CO_{3(aq)}$ was added until the solution reached a pH of 10. The solution was filtered and the filtrate was washed with water, dichloromethane, and diethyl ether. The filtrate was isolated and dried under vacuum to give ^{NMe2}**L** as an off-white solid (20% yield). ^{1}H NMR (500 MHz, CD_3OD) δ 7.49 (t, 2H, *p*-Py), 6.47 (d, 4H, *m*-Py), 5.94 (s, 2H, NMe_2-Py), 2.99 (s, 12H, NMe_2). $^{13}C\{^1H\}$ NMR (126 MHz, $CDCl_3$): δ 140.88, 133.45, 131.83, 129.99, 107.26, 91.93, 59.54.

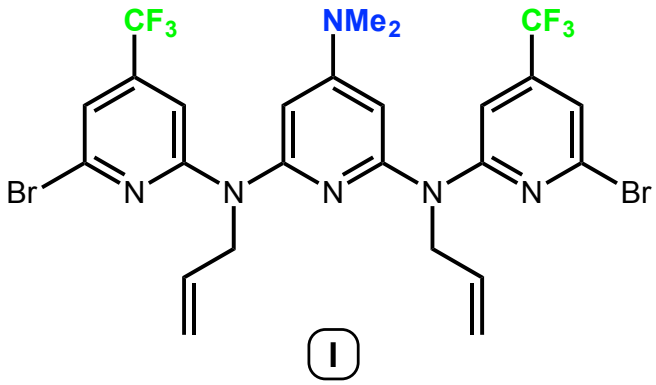

I

N2,N6-diallyl-N2,N6-bis(6-chloro-4-(trifluoromethyl)pyridin-2-yl)-N4,N4-dimethylpyridine-2,4,6-triamine (I), NaH (60 wt% in paraffin oil, 700 mg, 18.0 mmol) and **E** (700 mg, 3.00 mmol) were added to a stir bar equipped, oven dried 100 mL 3-neck flask under nitrogen atmosphere. THF (30 mL) was slowly added to generate an amber suspension. The mixture was then refluxed at 80 °C for one hour and was then taken off heat and allowed to cool. 2,6-dichloro-4-(trifluormethyl)pyridine (2.25 g, 10.4 mmol) was added to the mixture and the solution was brought back to reflux for 1 hour. The solution was cooled to room temperature and slowly quenched with cold water. The solvent was removed under vacuum and the residue was dissolved in dichloromethane (50 mL). The organic layer was washed with water (3 × 100 mL), dried with Na_2SO_4 and concentrated under vacuum to give a brown oil. The oil was chromotographed on a silica gel column with a 2:1 mixture of hexanes:ether as the mobile phase. The product was the first to elute. After removal of solvent the product is isolated as a yellow solid (65% yield). ^{1}H NMR (500 MHz, $CDCl_3$): δ 7.14 (s, 2H, *m*-CF_3-Py), 6.89 (s, 2H, *m*-CF_3-Py), 6.32 (s, 2H, outer *m*-NC_5H_2), 5.92 (m, 2H *H*C=CH_2), 5.17 (dd, 4H, HC=CH_2), 4.72 (m, 4H, H_2C-CH).

$^{13}C\{^{1}H\}$ NMR (126 MHz, $CDCl_3$): δ 157.83, 157.25, 150.10, 133.77, 116.72, 109.74, 106.42, 96.8, 51.07, 39.54. $^{19}F\{^{1}H\}$ NMR (470 MHz, $CDCl_3$) δ –64.9.

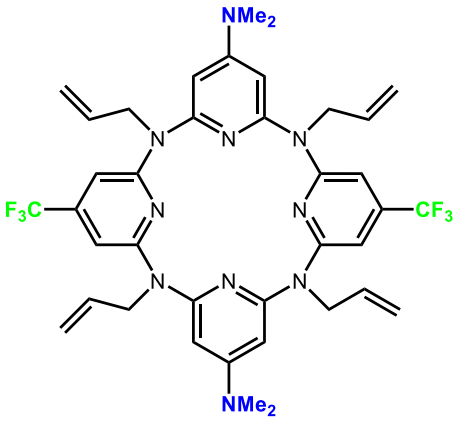

J

2,4,6,8-tetraallyl-N^1_4,N^1_4,N^5_4,N^5_4-tetramethyl-34,75-bis(trifluoromethyl)-2,4,6,8-tetraaza-1,3,5(2,6)-tripyridina-7(1,3)-benzenacyclooctaphane-14,54-diamine (J) $Pd_2(dba)_3$ (137.8 mg, 0.15 mmol), 1,3-Bis(diphenylphosphino)propane (124 mg, 0.30 mmol), and sodium *tert*-butoxide (300 mg, 3.12 mmol) were added to a stir bar equipped, oven dried 500 mL 3-neck flask under nitrogen protection. Dry toluene (250 mL) was syringed into the flask and the resultant red mixture was heated to 60 °C, when **E** (591.2 mg, 3.09 mmol) and **F** (232 mg, 1.00 mmol) were added to the suspension, causing a darkening in color. The reaction mixture was further heated to 110 °C and refluxed for one hour. After cooling to room temperature, the solvent was removed under reduced pressure and redissolved in dichloromethane (20 mL). The solution was washed with water (3 × 30 mL). The organic layers were dried with Na_2SO_4 and eluted through a 2:1 hexane:ether column (last spot to elute collected) followed by a 1:1:1 hexane:ether:dichloromethane column (first sport collected) to give **G** as an off-white solid (30% yield). **Note: this was not fully purified as evident from the NMR spectra. We believe that the impurities are various isomers in which the allyl bond is isomerized. These impurities do not inhibit subsequent synthetic steps.** ^{1}H NMR (500 MHz, $CDCl_3$) δ 6.15 (s, 4H, *m*-CF_3-Py), 6.04 (s, 4H, *m*-NMe_2-Py), 5.91 (m, 4H, *H*C=CH_2), 5.33-5.14 (dd, 8H, HC=C*H*$_2$), 4.38-4.12 (dd, 8H, *H*$_2$C-CH), 2.89 (s, 12H, N(C*H*$_3$)$_2$). $^{13}C\{^{1}H\}$ NMR (126 MHz, $CDCl_3$) δ158.42, 134.38, 115.89, 104.87, 91.78, 52.54. $^{19}F\{^{1}H\}$ NMR (470 MHz, $CDCl_3$) δ –68.92 (s, 6F, CF_3).

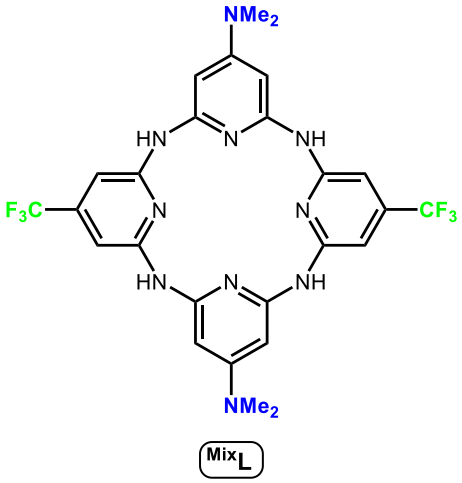

(NH)$_4$-BridgedCalix[4]-pyridine (Py$_4$(NMe$_2$)$_2$(CF$_3$)$_2$NH$_4$) (^{Mix}L), $Pd_2(dba)_3$ (7.0 mg, 0.008 mmol), 1,1'-Bis(diphenylphosphino)ferrocene (5.5 mg 0.010 mmol), and potassium *tert*-butoxide (55 mg 0.49 mmol) were added to a stir bar equipped, oven dried 100 mL 3-neck flask under nitrogen atmosphere. Dry toluene (100 mL) was syringed into the flask and the resultant red mixture was heated. Upon reaching approximately 60 °C, **C** (56.9 mg, 0.074 mmol), was added to the suspension, causing a darkening in color. The reaction mixture was heated to 110 °C and refluxed for one hour. After cooling to room temperature, the solvent was removed under reduced pressure and redissolved in diethyl ether (20 mL). The solution was washed with water (3 × 30 mL). The organic layers were dried with Na_2SO_4 and filtered through a 2.5 cm × 1 cm silica containing fritted glass funnel. The resultant organic fraction was reduced under pressure to give brown oil. The oil was dissolved in a 10:1 acetone:water mixture (10 mL) and excess concentrated hydrochloric acid was added. The resultant orange mixture was heated to reflux for an hour. The acetone was removed under reduced pressure and $Na_2CO_{3(aq)}$ was added until the solution reached a pH of 10. The solution was filtered and the filtrate was washed with benzene. The filtrate was isolated and dried under vacuum to give **D** as an off-white solid (85% yield). ^{1}H NMR (500 MHz, acetone-d_6): δ 7.94 (s, 4H, N*H*), 6.42 (s, 4H, *m*-CF$_3$-Py), 6.00 (s, 4H, *m*-NMe$_2$-Py), 2.93 (s, 12H, N(C*H*$_3$)$_2$). ^{13}C{^{1}H} NMR (126 MHz, $CDCl_3$): δ 13.50, 129.46, 129.39, 88.20, 77.18, 64.04, 24.85. ^{19}F{^{1}H} NMR (470 MHz, $CDCl_3$) δ –65.75.

NMR Spectra

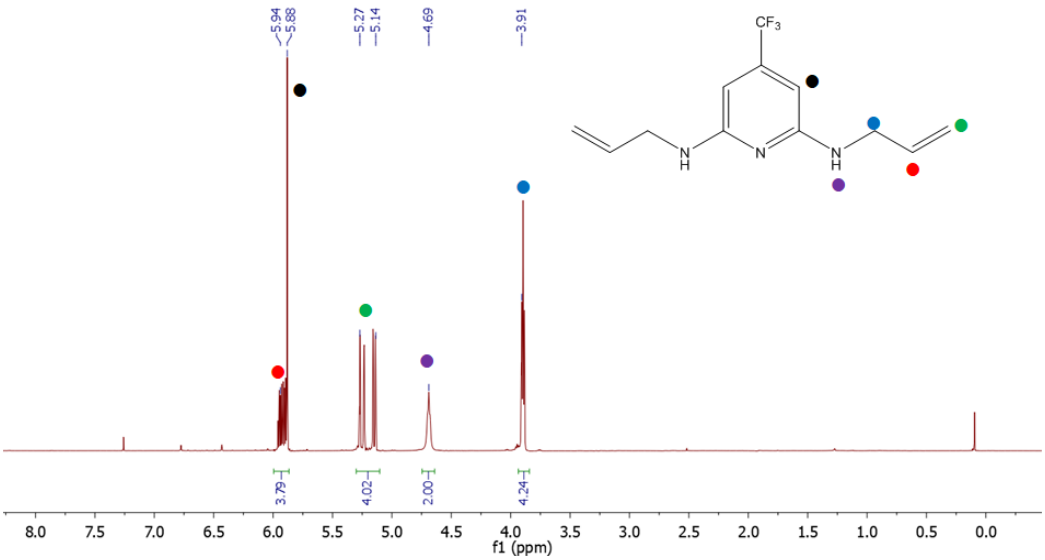

Figure S20. 500 MHz ^{1}H NMR spectrum of **B** in $CDCl_3$.

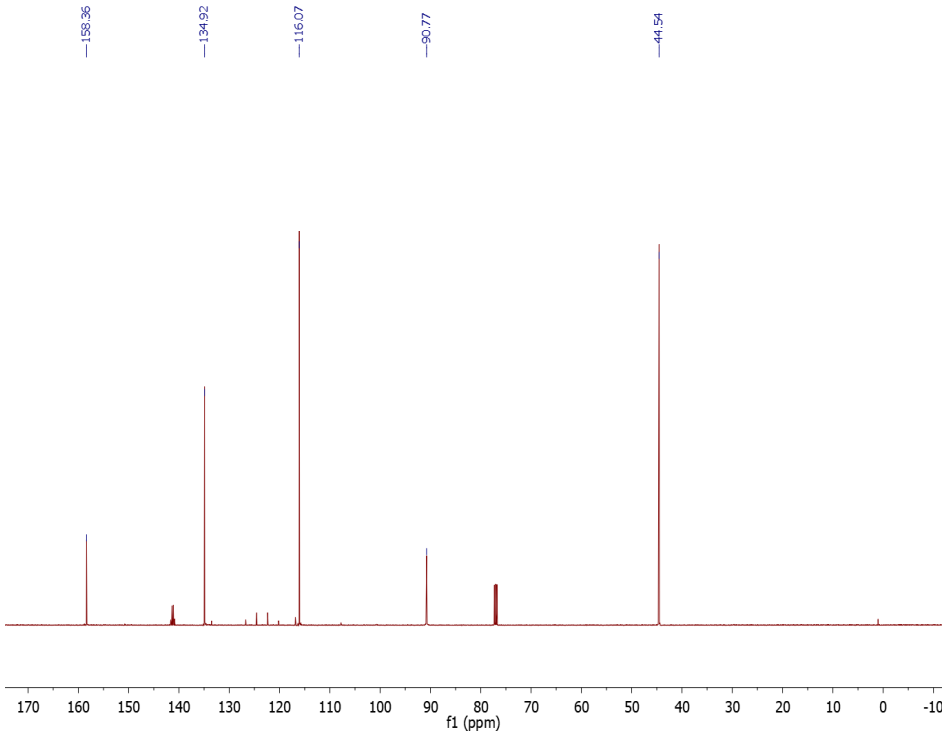

Figure S21. 126 MHz $^{13}C\{^{1}H\}$ NMR spectrum of **B** in $CDCl_3$.

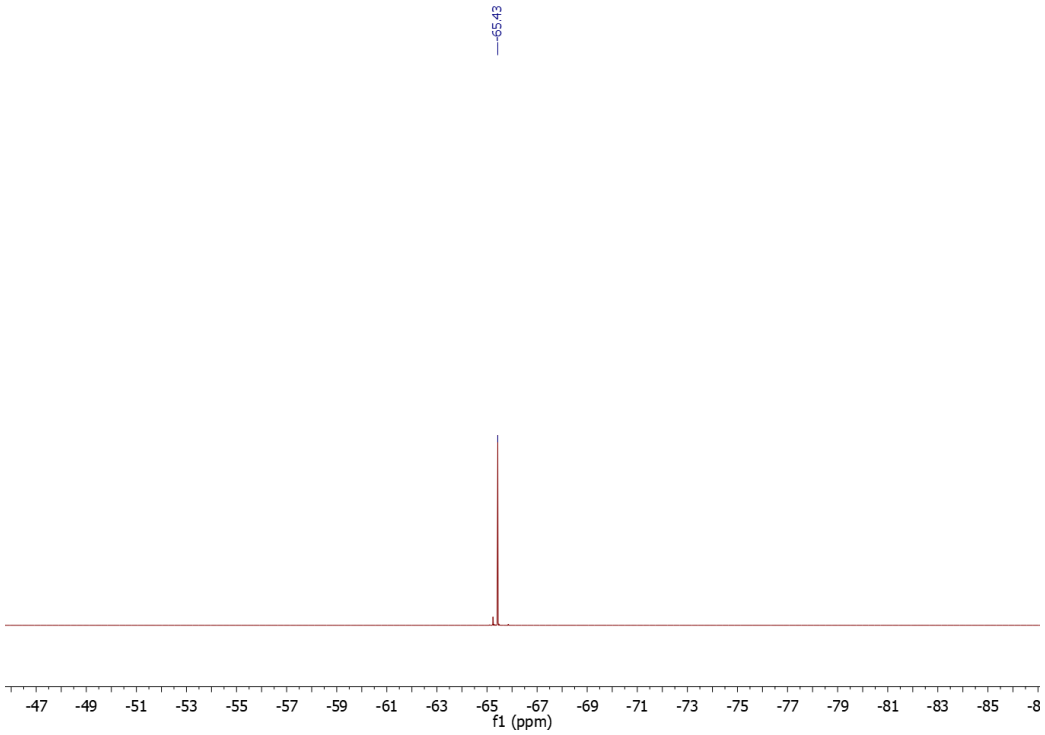

Figure S22. 470 MHz $^{19}F\{^{1}H\}$ NMR spectrum of **B** in $CDCl_3$.

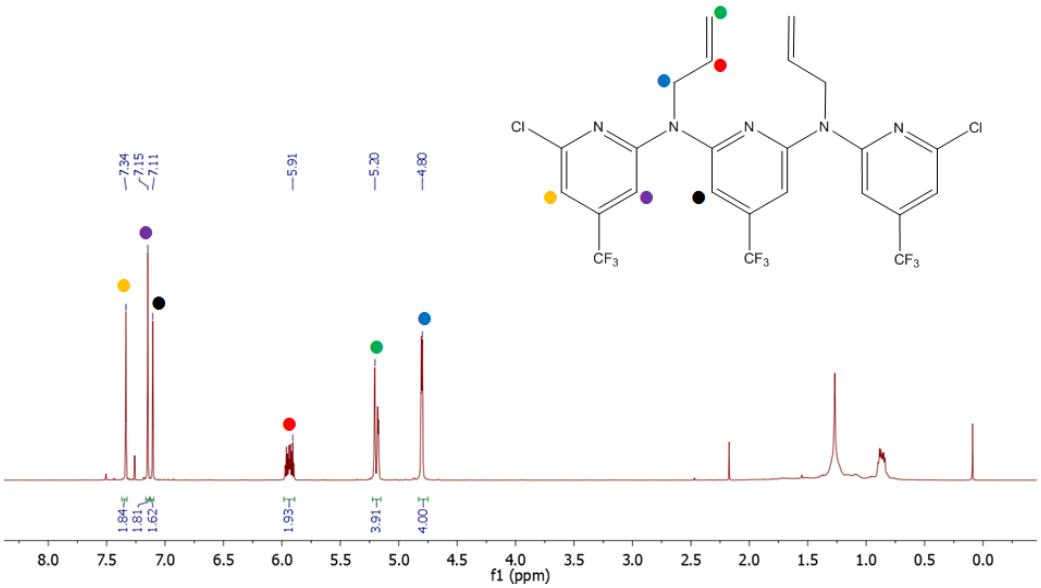

Figure S23. 500 MHz ^{1}H NMR spectrum of **C** in $CDCl_3$.

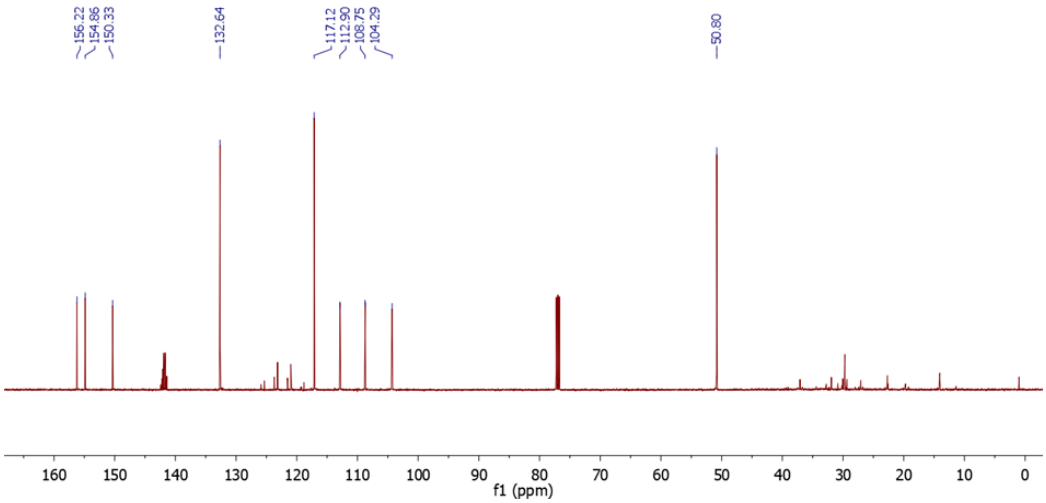

Figure S24. 126 MHz $^{13}C\{^{1}H\}$ NMR spectrum of **C** in $CDCl_3$.

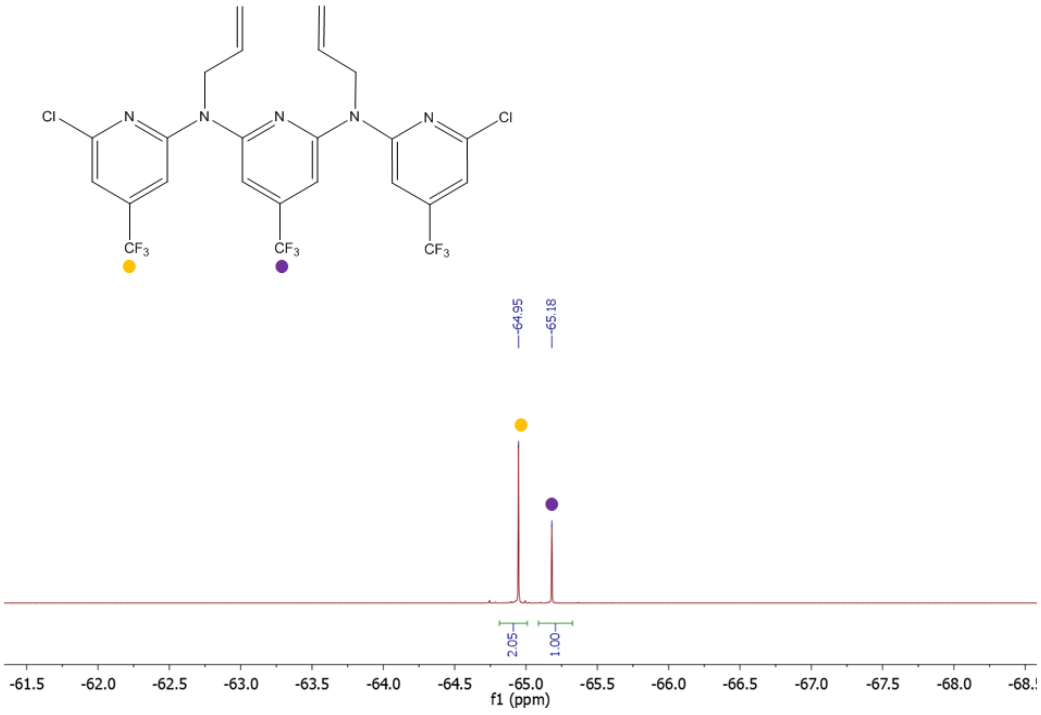

Figure S25. 470 MHz $^{19}F\{^{1}H\}$ NMR spectrum of **C** in $CDCl_3$.

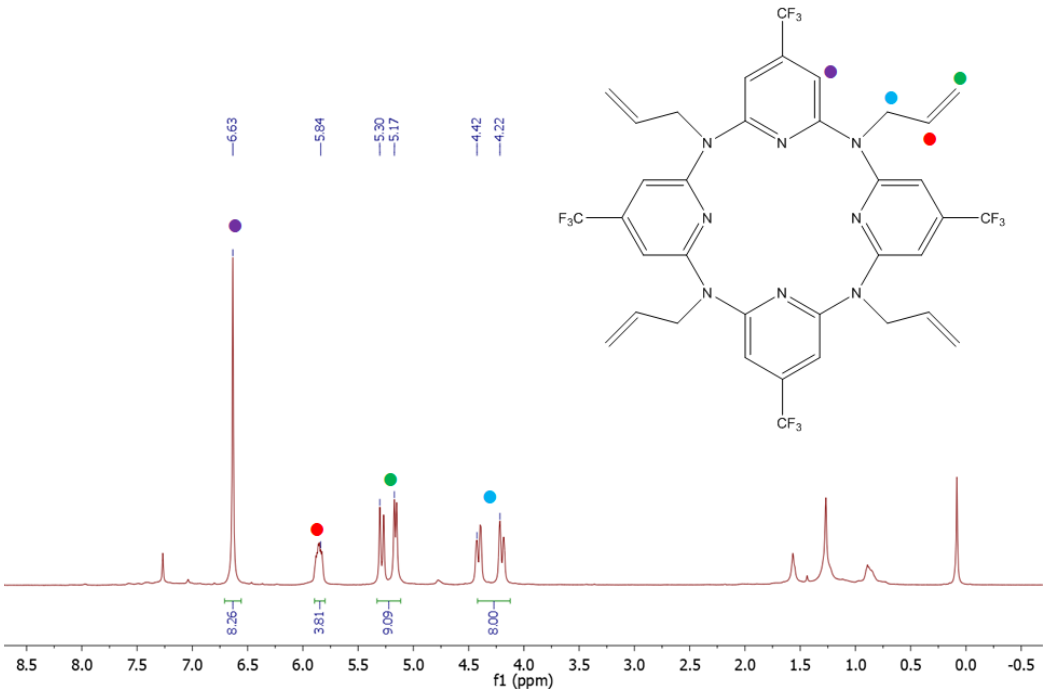

Figure S26. 500 MHz ^{1}H NMR spectrum of **D** in $CDCl_3$.

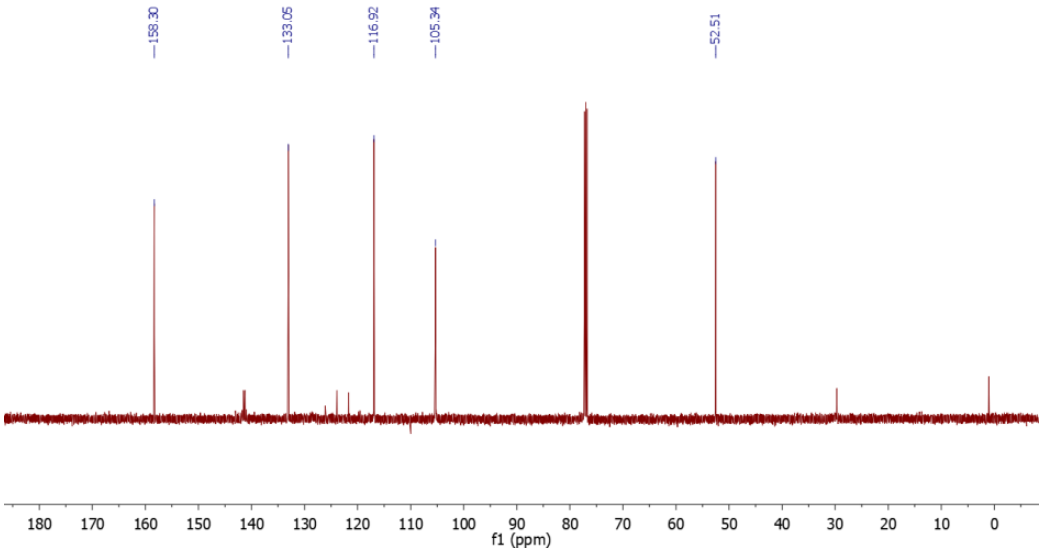

Figure S27. 126 MHz $^{13}C\{^{1}H\}$ NMR spectrum of **D** in $CDCl_3$.

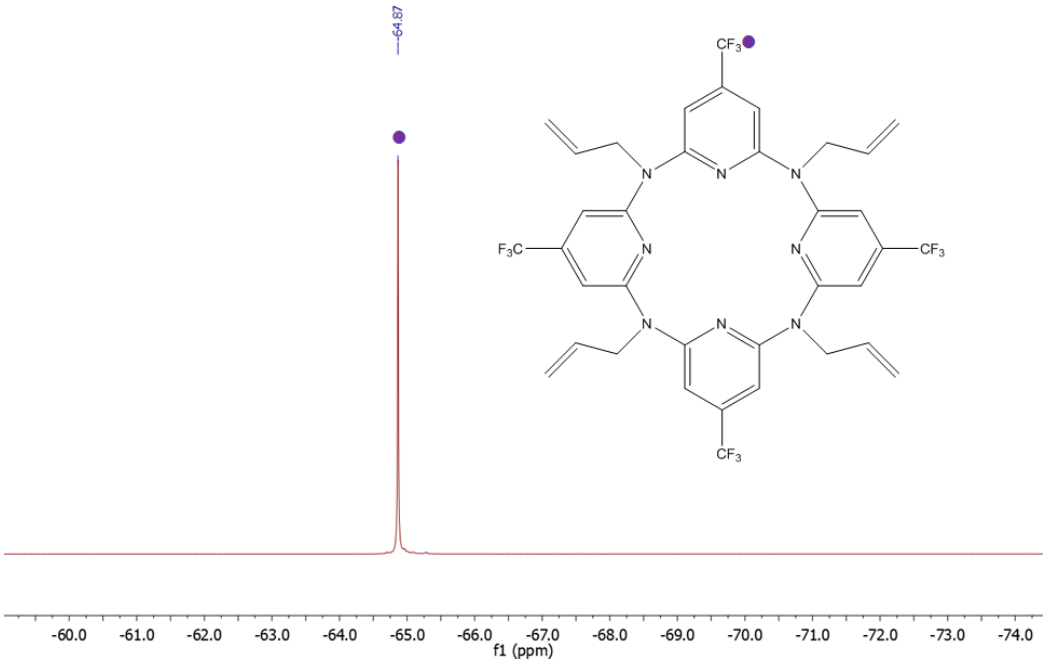

Figure S28. 470 MHz $^{19}F\{^{1}H\}$ NMR spectrum of **D** in $CDCl_3$.

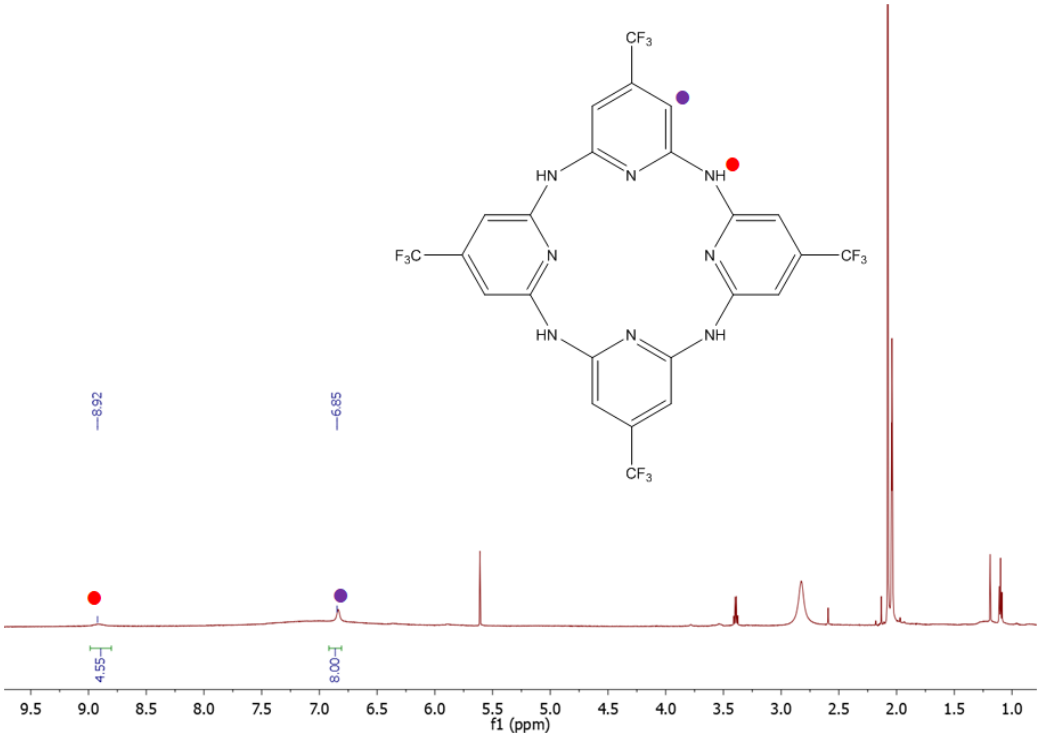

Figure S29. 500 MHz ^{1}H NMR spectrum of ^{CF3}**L** in acetone-d_6.

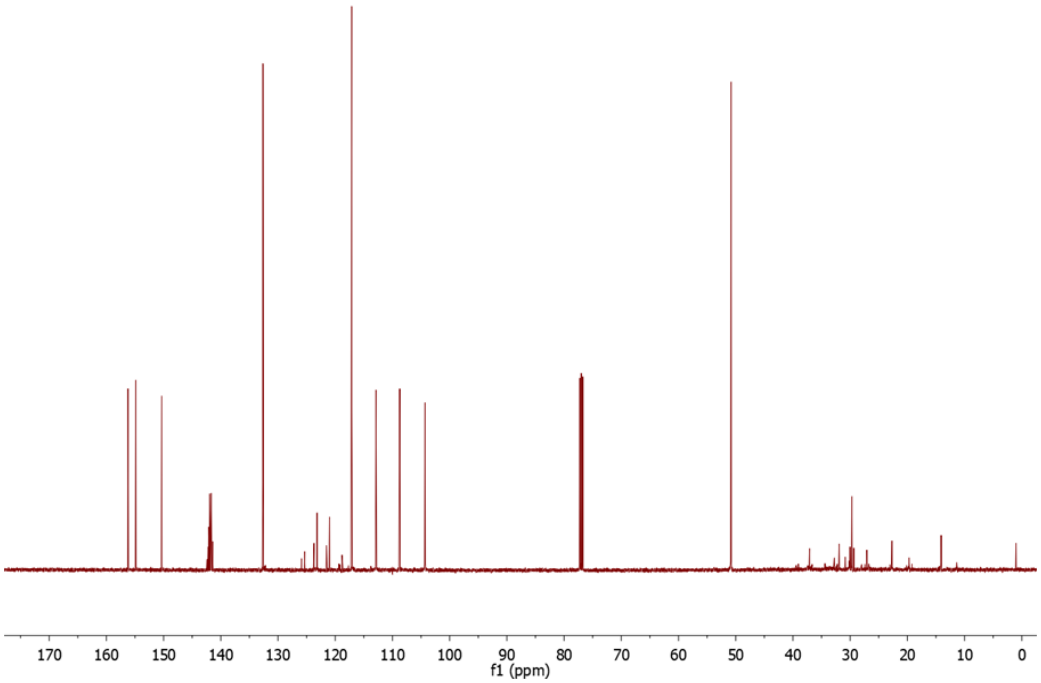

Figure S30. 126 MHz $^{13}C\{^{1}H\}$ NMR spectrum of ^{CF3}**L** in acetone-d_6.

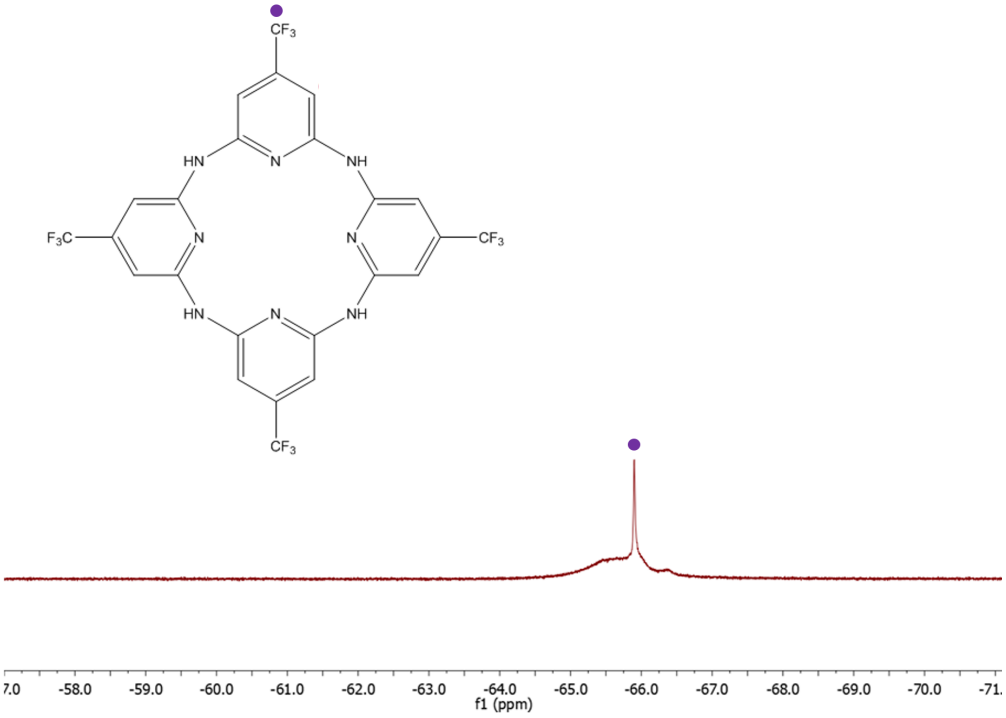

Figure S31. 470 MHz $^{19}F\{^{1}H\}$ NMR spectrum of ^{CF3}**L** in acetone-d_6.

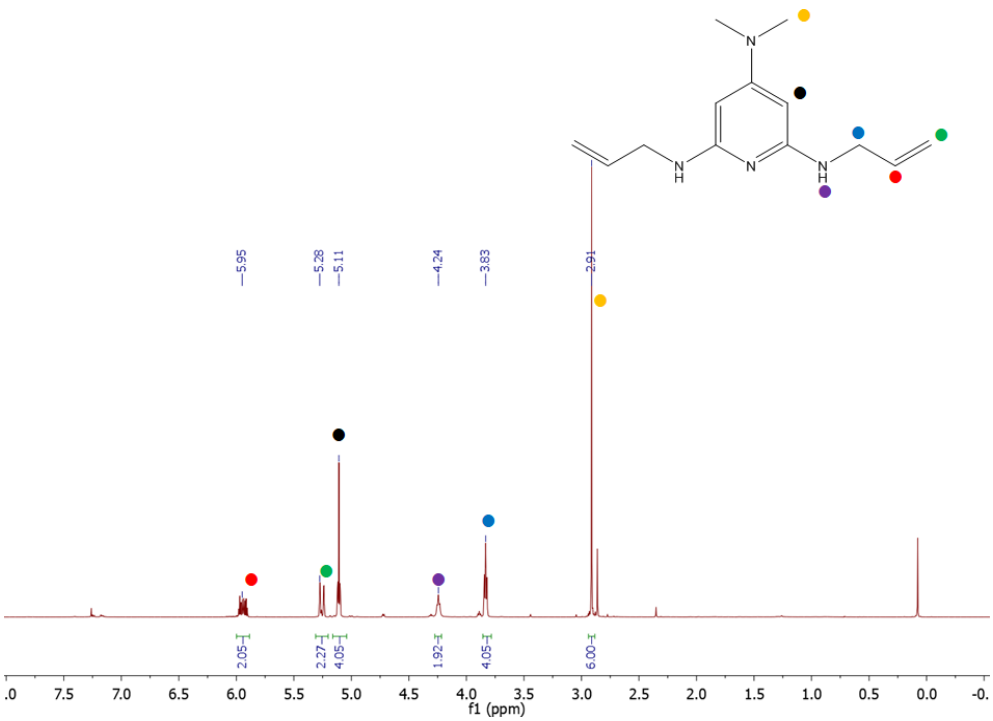

Figure S32. 500 MHz ^{1}H NMR spectrum of **F** in $CDCl_3$.

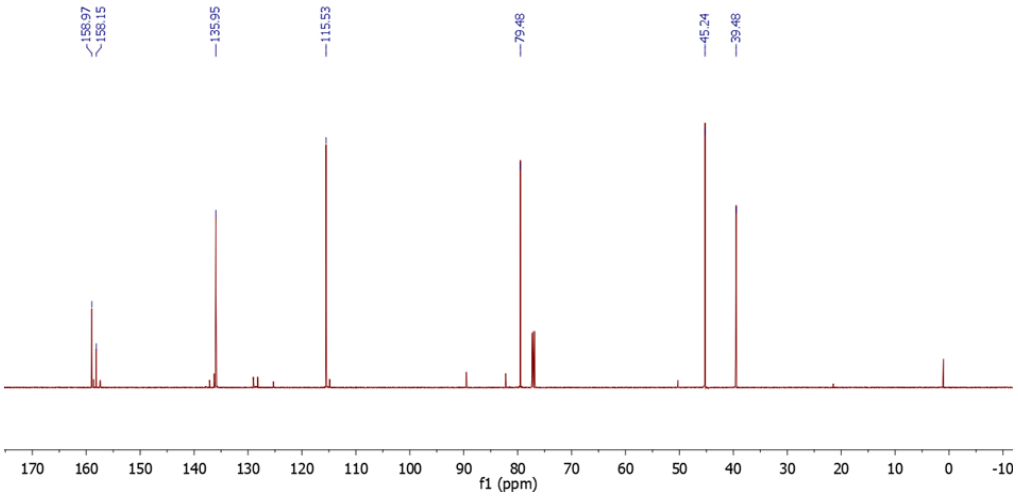

Figure S33. 126 MHz $^{13}C\{^{1}H\}$ NMR spectrum of **F** in $CDCl_3$.

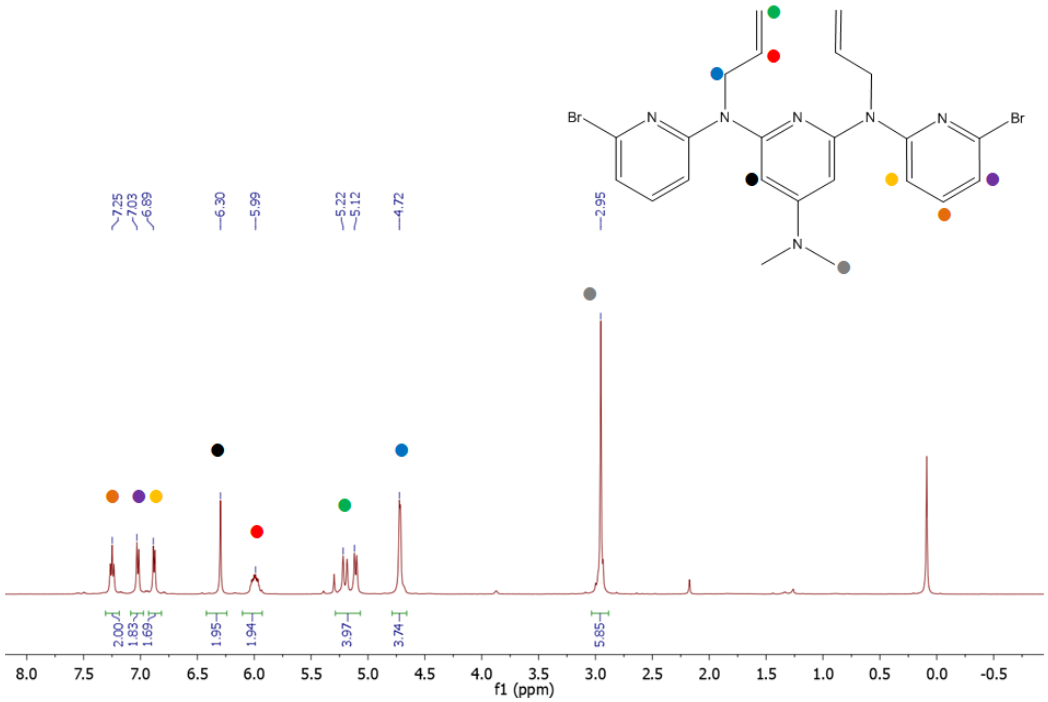

Figure S34. 500 MHz ^{1}H NMR spectrum of **G** in $CDCl_3$.

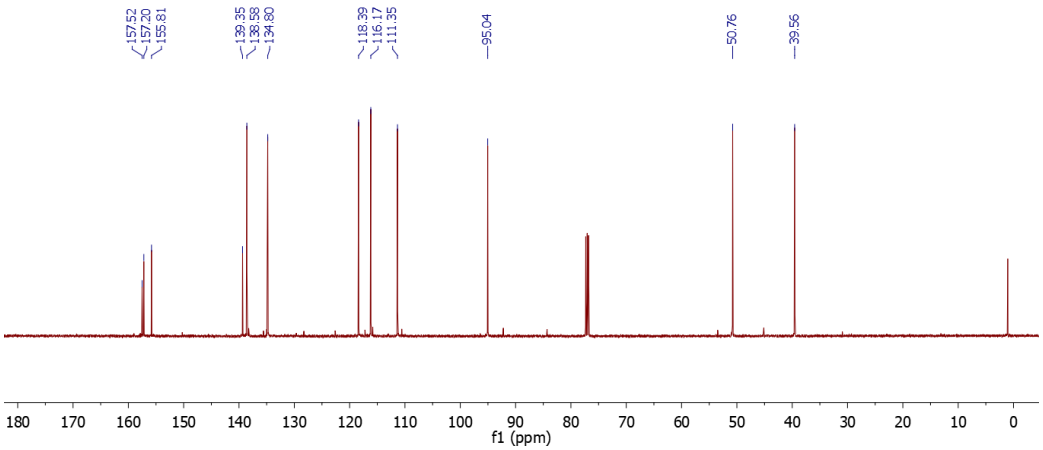

Figure S35. 126 MHz ^{13}C{^{1}H} NMR spectrum of **G** in $CDCl_3$.

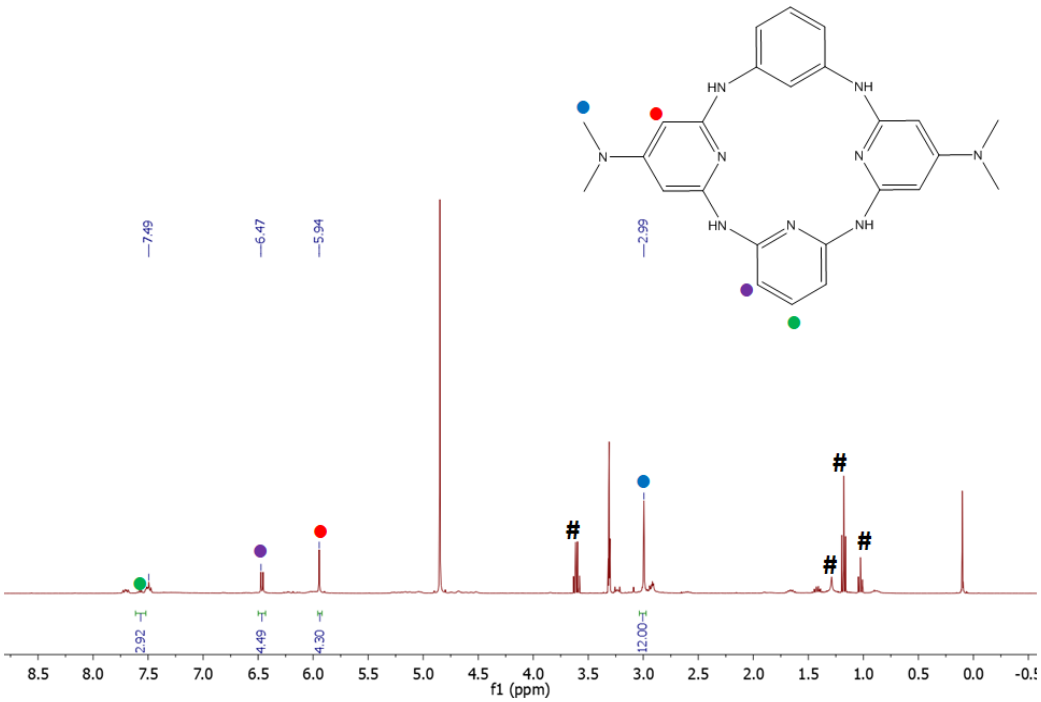

Figure S36. 500 MHz ^{1}H NMR spectrum of $^{\mathbf{NMe2}}$**L** in CD_3OD. Adventitious solvent peaks are designated with a hash (#) symbol.

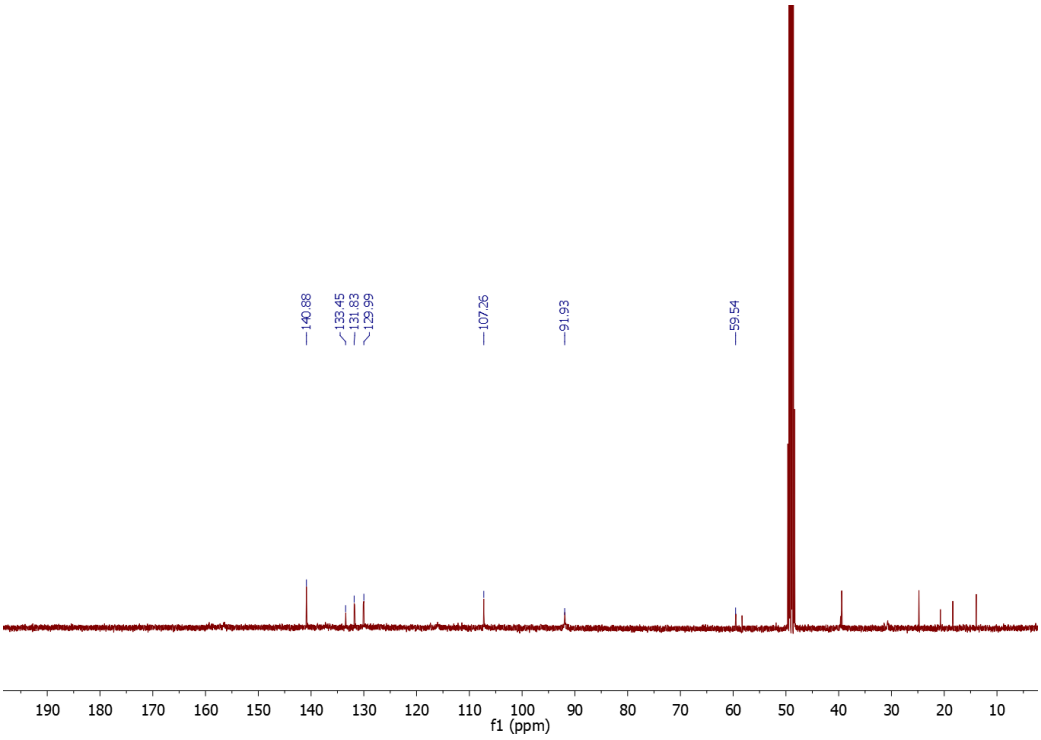

Figure S37. 126 MHz $^{13}C\{^{1}H\}$ NMR spectrum of $^{\mathbf{NMe2}}$**L** in CD_3OD.

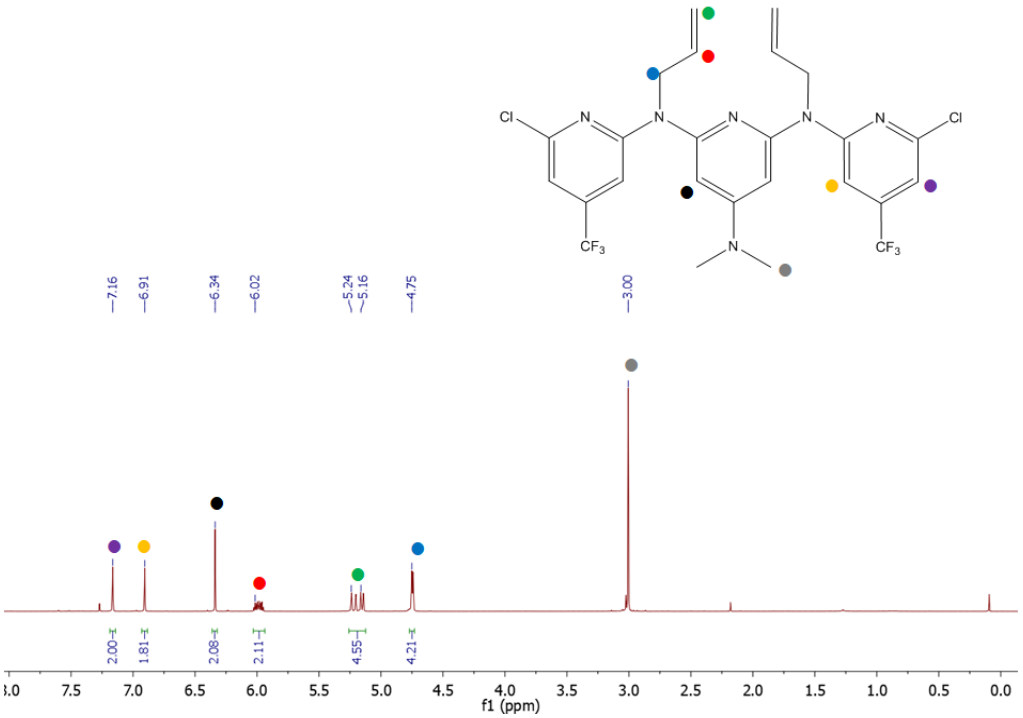

Figure S38. 500 MHz ^{1}H NMR spectrum of **I** in $CDCl_3$.

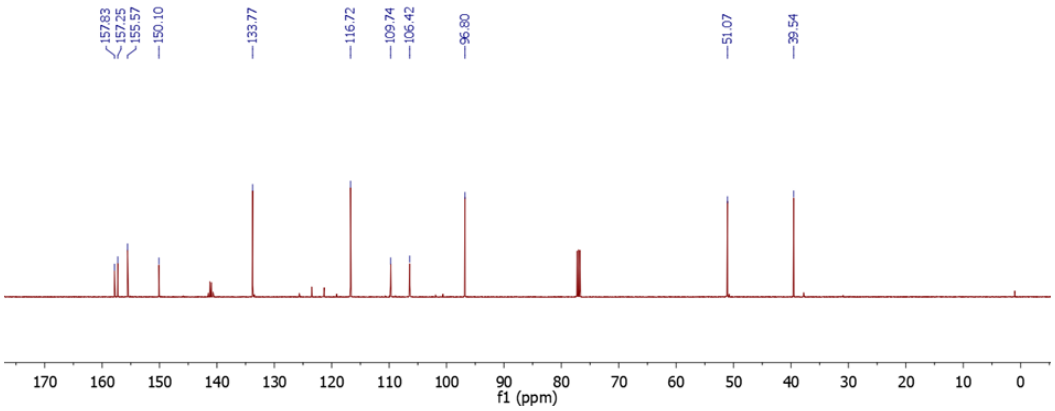

Figure S39. 126 MHz ^{13}C{^{1}H} NMR spectrum of **I** in $CDCl_3$.

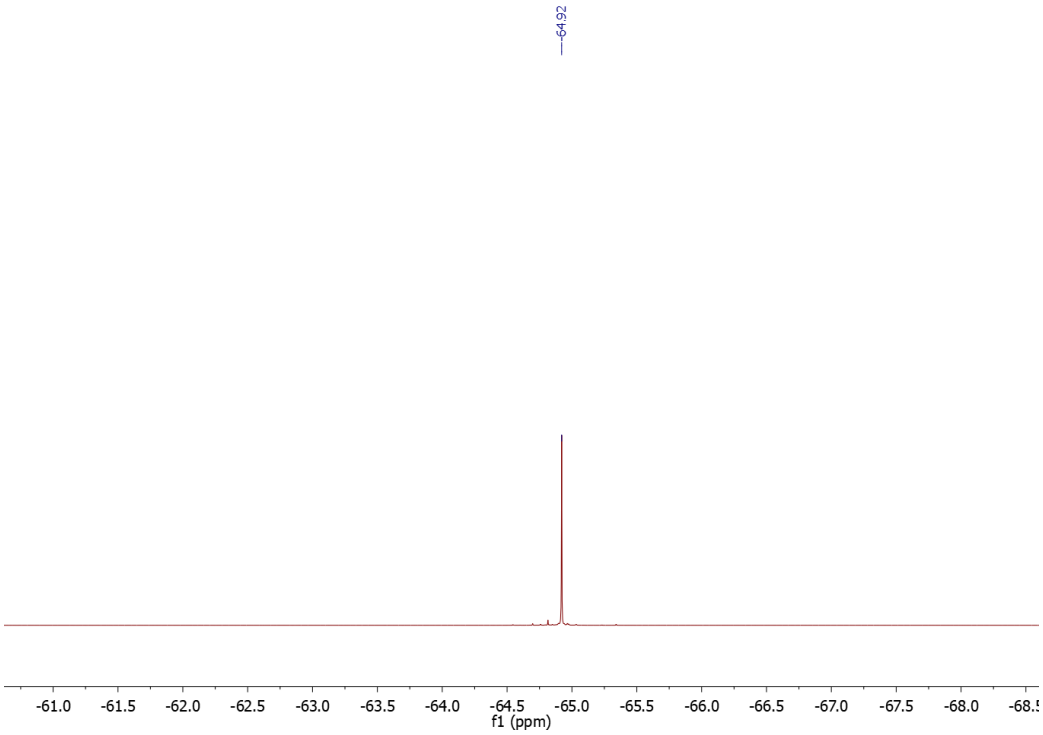

Figure S40. 470 MHz $^{19}F\{^{1}H\}$ NMR spectrum of **I** in $CDCl_3$.

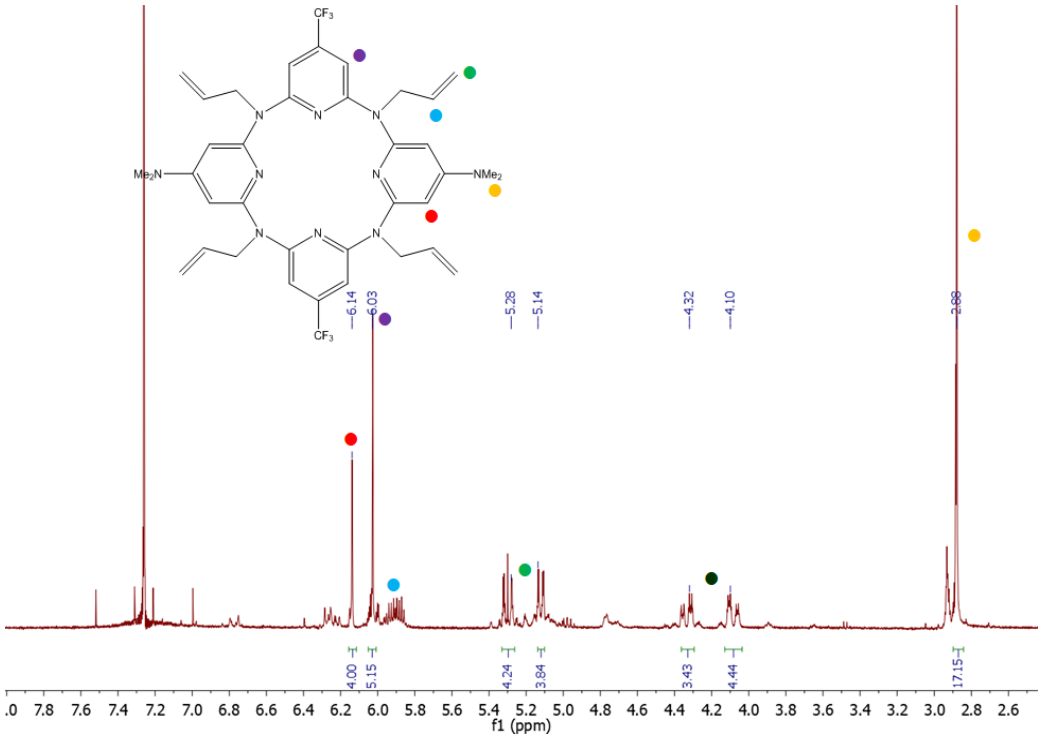

Figure S41. 500 MHz ^{1}H NMR spectrum of **J** in $CDCl_3$. The impurities in the spectrum correspond to cycles bearing isomerized allyl groups.

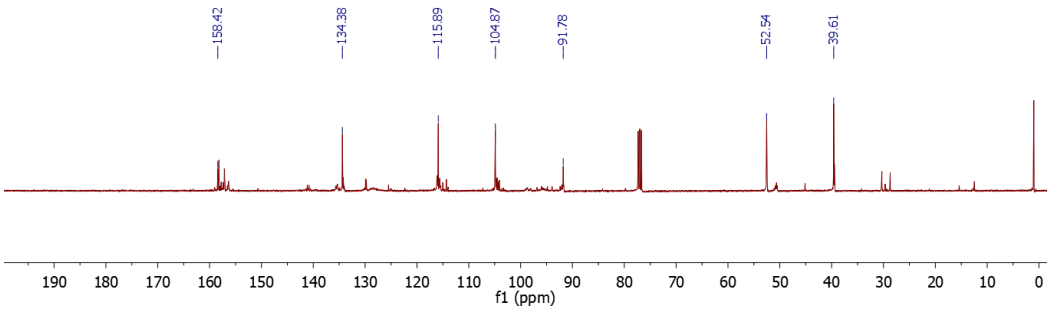

Figure S42. 126 MHz $^{13}C\{^{1}H\}$ NMR spectrum of **J** in $CDCl_3$.

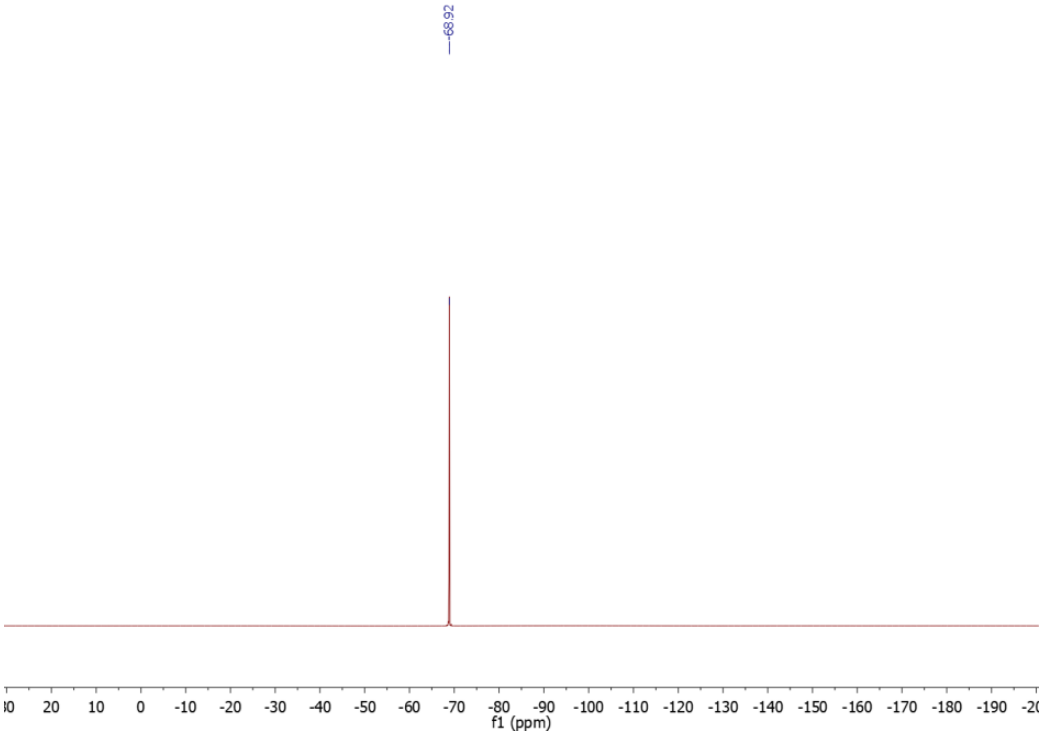

Figure S43. 470 MHz $^{19}F\{^{1}H\}$ NMR spectrum of **J** in $CDCl_3$.

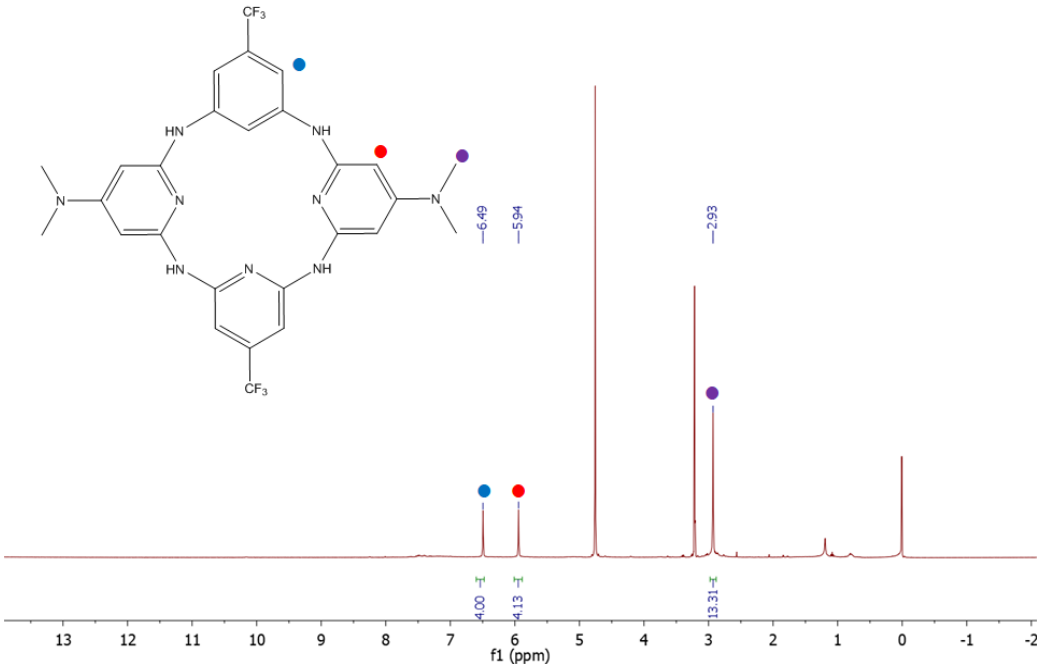

Figure S44. 500 MHz ^{1}H NMR spectrum of $^{\mathbf{Mix}}$**L** in CD_3OD.

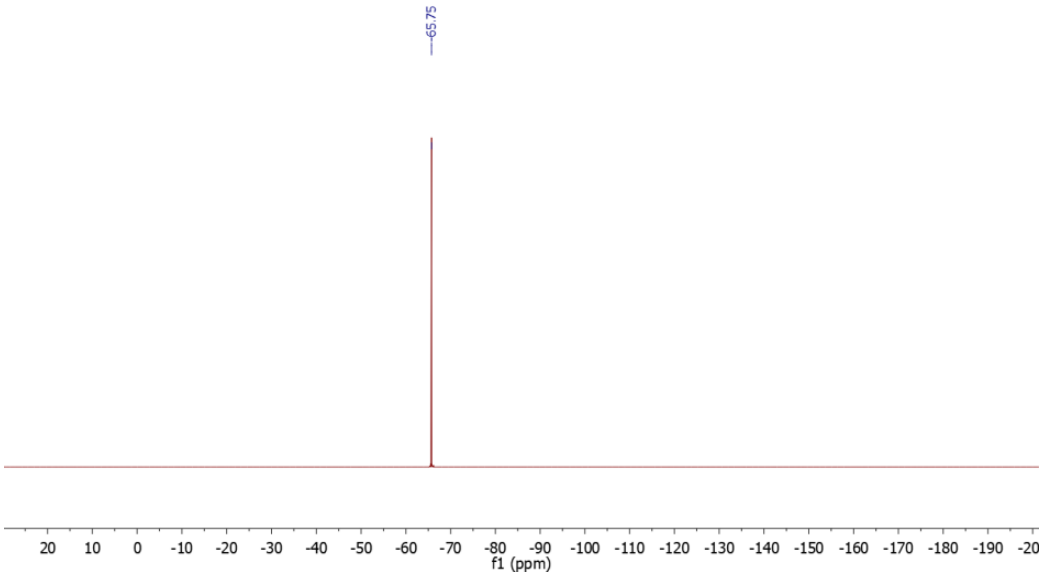

Figure S45. 470 MHz ^{19}F{^{1}H} NMR spectrum of $^{\mathbf{Mix}}$**L** in CD_3OD.

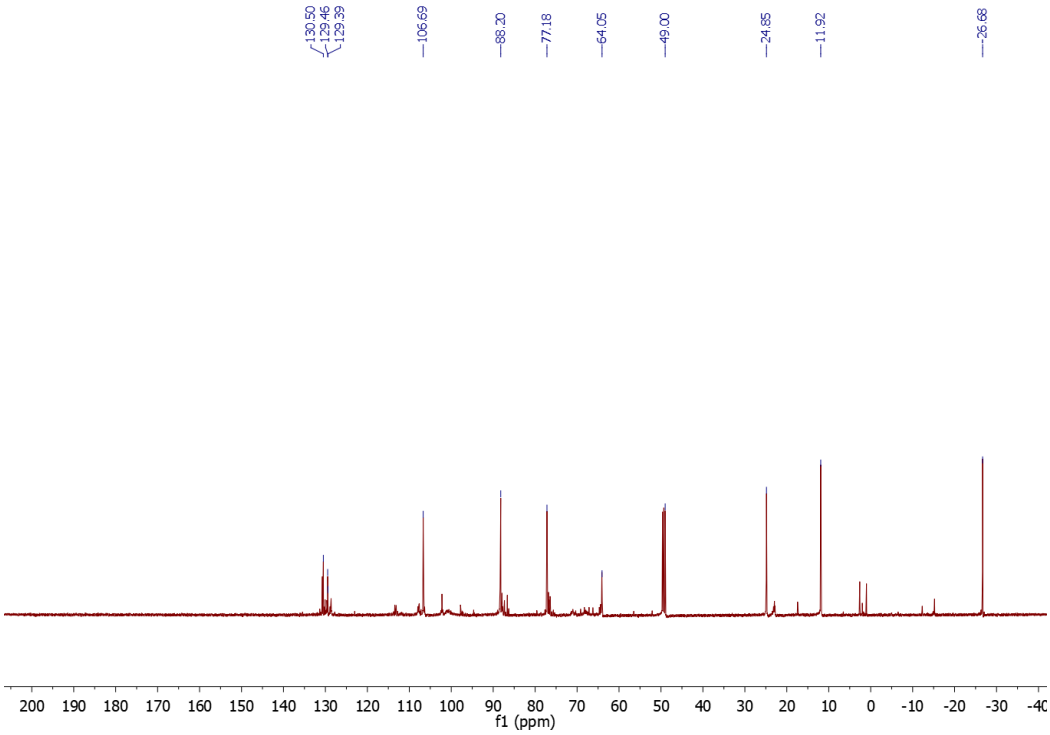

Figure S46. 126 MHz $^{13}C\{^{1}H\}$ NMR spectrum of $^{\mathbf{Mix}}\mathbf{L}$ in CD_3OD.

Evans Method Experiments

In a scintillation vial, a pre-weighted quantity of the cobalt complex (5.6, 3.1, 3.6, and 1.1 mg for complexes **1**–**3**, and **4–Cl**, respectively) was dissolved in 0.7 mL DMSO-d_6. The solution was transferred to an NMR tube and a sealed capillary containing pure DMSO-d_6 was inserted into the cobalt solution. A ^{1}H NMR spectrum was then collected on a 500 MHz spectrometer at 298 K. The corrected molar susceptibility (X_P) was calculated based on the shift of the residual solvent resonances in the solution of the complex *vs*. that found in the internal capillary using the equation below where Δf is the observed ^{1}H NMR shift of the reference standard in Hz, C is the concentration of the sample in mol/L, f is the proton Larmor frequency (500,000,000 Hz), and X_D is the diamagnetic susceptibility correction factor (calc. –4.32 x 10^{-5} μ_B).

$$X_P = \frac{3000 \times \Delta f}{4\pi C f} - X_D$$

The effective magnetic moment was calculated using the equation below where T is the temperature in Kelvin, X_P is the corrected molar susceptibility, and μ_{eff} is the effective magnetic moment in Bohr Magnetons.

$$\mu_{eff} = 2.84\sqrt{T \times X_P}$$

The observed magnetic moments for complexes **2**–**4** (4.78, 4.52 and 4.97 μ_B, respectively) are consistent with a high-spin Co^{2+} center (d^7, S = 3/2) possessing three unpaired spins. The same result was found for the unsubstituted cobalt aminopyridine complex, **1** (*ACS Cent. Sci.*, **2018**, *4*, 397-404).

Table S6. Summary of Evans method experiments for complexes **1**–**4**. All experiments were conducted in DMSO–d_6 solvent at 298 K and in a 500 MHz spectrometer. Measured magnetic moments fall in the range expected for a S = 3/2 Co^{2+} complex.[19]

Complex	[Co] (mM)	Δf (Hz)	μ_{eff} (μ_B)
1	10.8	223.5	4.98
2	4.6	87.5	4.78
3	6.1	103.0	4.52
4–Cl	1.6	33.0	4.97

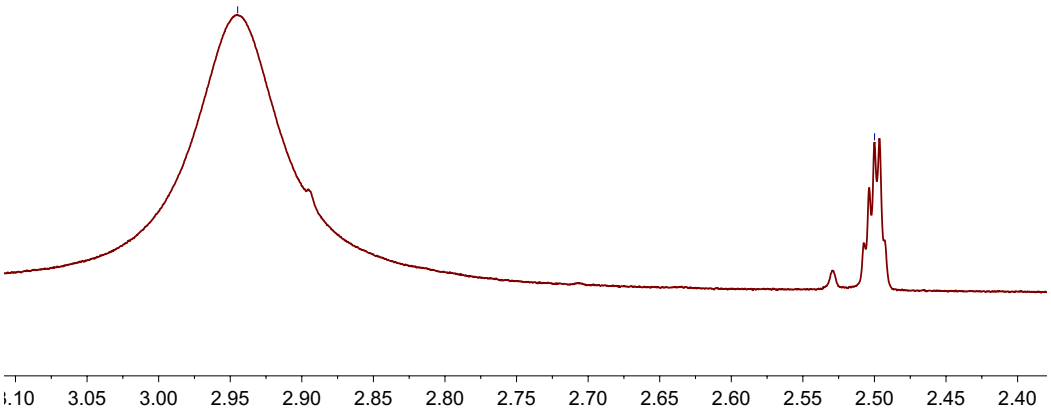

Figure S47. Selected region of the ^{1}H NMR (500 MHz) spectrum of complex **1** in DMSO-d_6 showing the paramagnetic shift of the residual solvent resonance ([Co] = 10.8 mM; Δf = 223.5 Hz).

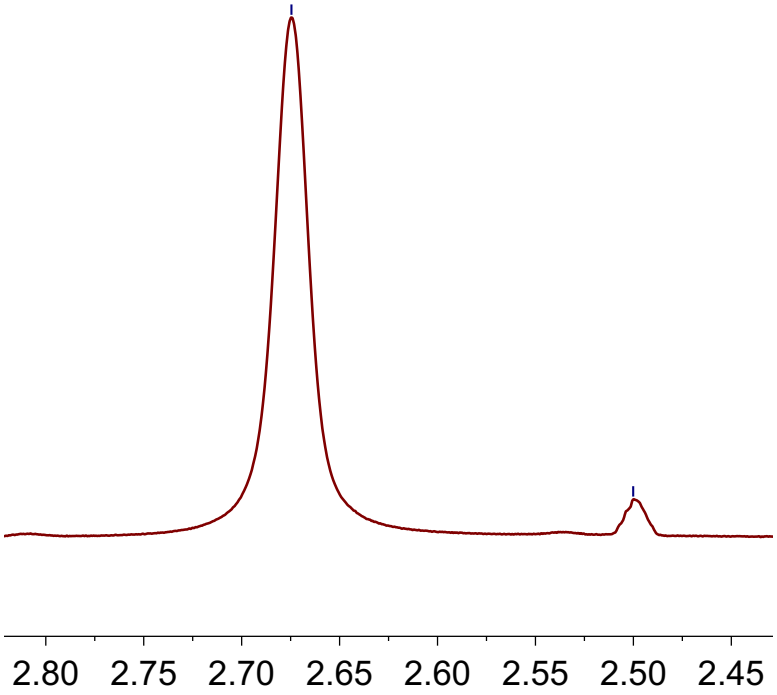

Figure S48. Selected region of the ^{1}H NMR (500 MHz) spectrum of complex **2** in DMSO-d_6 showing the paramagnetic shift of the residual solvent resonance ([Co] = 4.6 mM; Δf = 87.5 Hz).

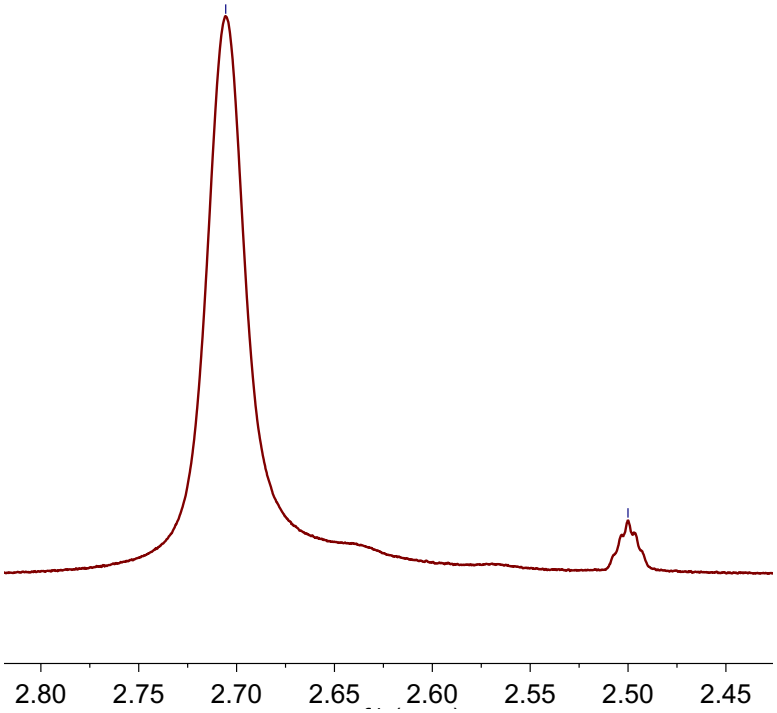

Figure S49. Selected region of the ^{1}H NMR (500 MHz) spectrum of complex **3** in DMSO-d_6 showing the paramagnetic shift of the residual solvent resonance ([Co] = 6.1 mM; Δf = 103.0 Hz).

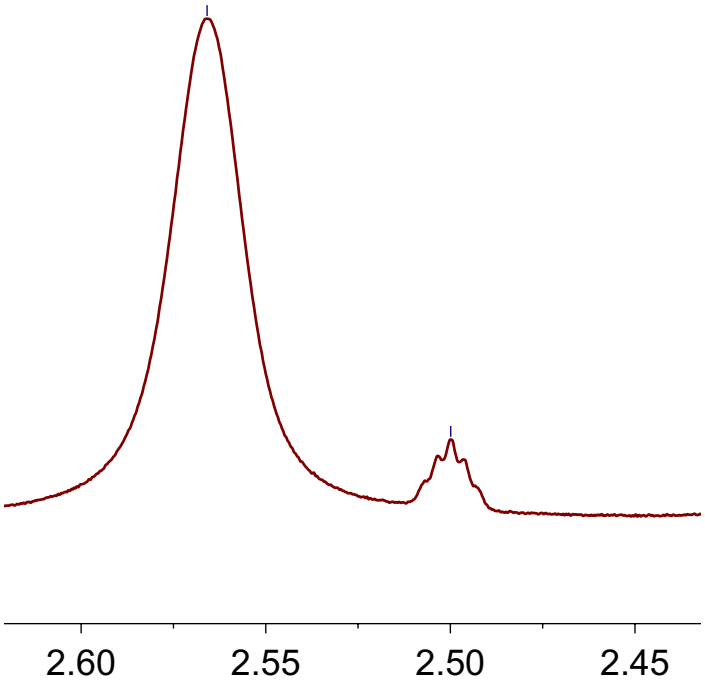

Figure S50. Selected region of the ^{1}H NMR (500 MHz) spectrum of complex **4–Cl** in DMSO-d_6 showing the paramagnetic shift of the residual solvent resonance ([Co] = 1.6 mM; Δf = 33.0 Hz).

High Scan Rate Cyclic Voltammetry for Complex 2

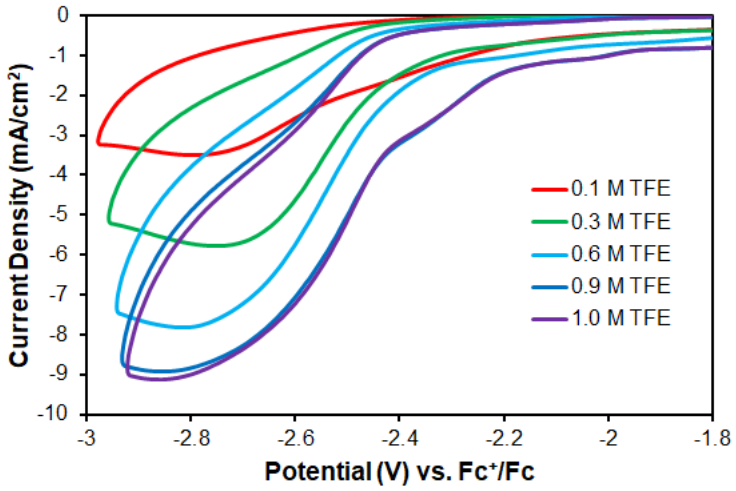

Figure S51. Cyclic Voltammetry of complex **2** (0.5 mM) in a DMF solution containing 0.1 M [*n*Bu$_4$N][PF$_6$] under CO_2 atmosphere with varying amounts of TFE at 2000 mV/s scan rate.

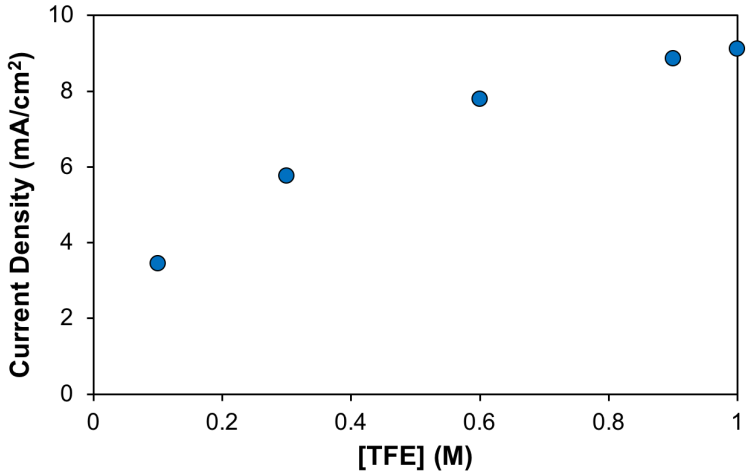

Table S7. Catalytic current for the titration of complex **2** with TFE at ν = 2000 mV/s.

[TFE] (M)	i_{cat} (mA/cm^2)
0.1	3.45
0.3	5.76
0.6	7.8
0.9	8.87
1	9.123

Supplementary Cyclic Voltammetry Titration Data

All Titrations with TFE were performed under 1 atmosphere of CO_2 and [Co] = 0.5 mM (containing 0.1 M [nBu$_4$N][PF$_6$] electrolyte in DMF), utilizing glassy carbon working electrode, Pt wire counter electrode and Ag pseudo reference electrode.

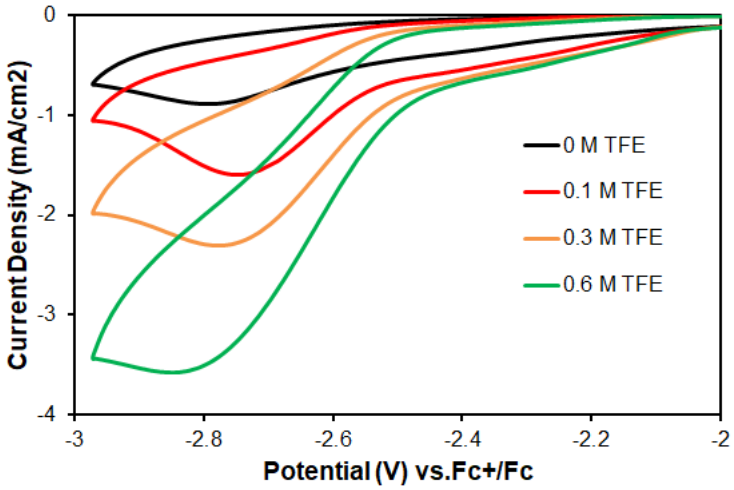

Figure S52. Cyclic Voltammetry of complex **2** (0.5 mM) in a DMF solution containing 0.1 M [nBu$_4$N][PF$_6$] under CO_2 atmosphere with varying amounts of TFE. Scans were collected at 100 mV/s.

Table S8. Catalytic current for the titration of complex **2** with TFE. i_p = 0.0177 mA/cm^2, extrapolated from the reversible Co$^{II/I}$ couple.

[TFE] (M)	i_{cat} (mA/cm^2)	i_{cat}/i_p
0.1	1.59	89.8
0.3	2.29	129.4
0.6	3.57	201.7

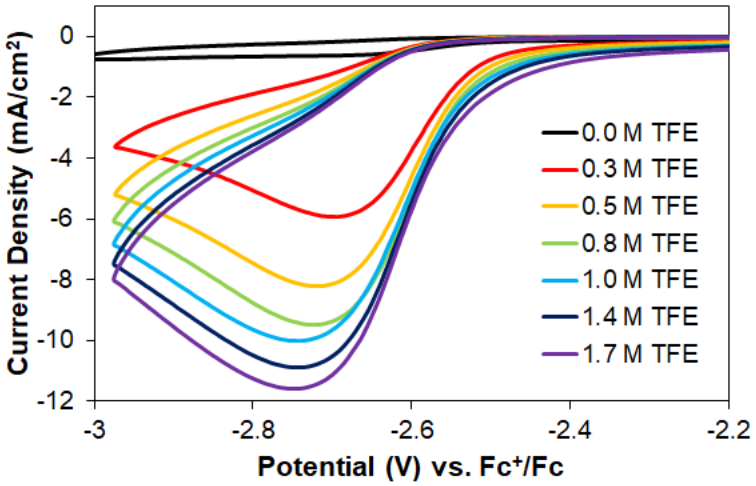

Figure S53. Cyclic Voltammetry of complex **3** (0.5 mM) in a DMF solution containing 0.1 M [*n*Bu$_4$N][PF$_6$] under CO_2 atmosphere with varying amounts of TFE. Scans were collected at 100 mV/s.

Table S9. Catalytic current for the titration of complex **3** with TFE. i_p = 0.0140 mA/cm^2, extrapolated from the reversible $Co^{II/I}$ couple.

[TFE] (M)	i_{cat} (mA/cm^2)	i_{cat}/i_p
0.3	5.92	423.8
0.5	8.22	588.4
0.8	9.45	676.4
1	9.98	714.0
1.4	10.85	776.5
1.7	11.59	829.8

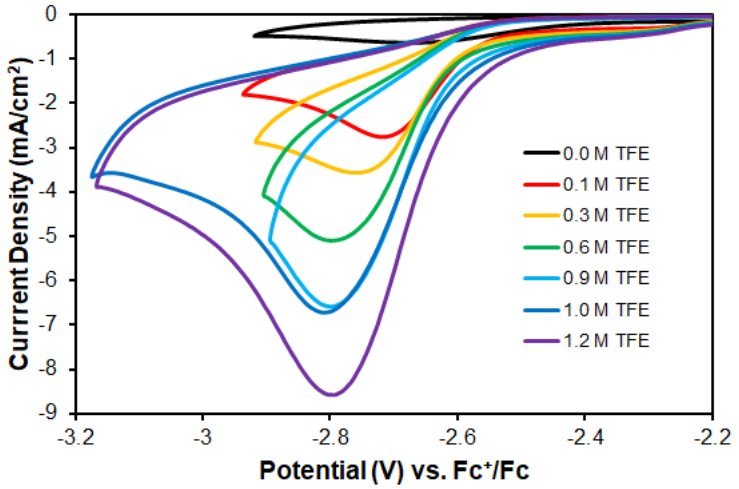

Figure S54. Cyclic Voltammetry of complex **4** (0.5 mM) in a DMF solution containing 0.1 M [*n*Bu$_4$N][PF$_6$] under CO_2 atmosphere with varying amounts of TFE. Scans were collected at 100 mV/s.

Table S10. Catalytic current for the titration of complex **4** with TFE. i_p = 0.0357 mA/cm^2, extrapolated from the reversible $Co^{II/I}$ couple.

[TFE] (M)	i_{cat} (mA/cm^2)	i_{cat}/i_p
0.1	2.76	77.3
0.3	3.57	99.9
0.6	5.09	142.6
0.9	6.58	184.5
1	6.69	187.4
1.2	8.54	239.3

Supplementary CPE Data

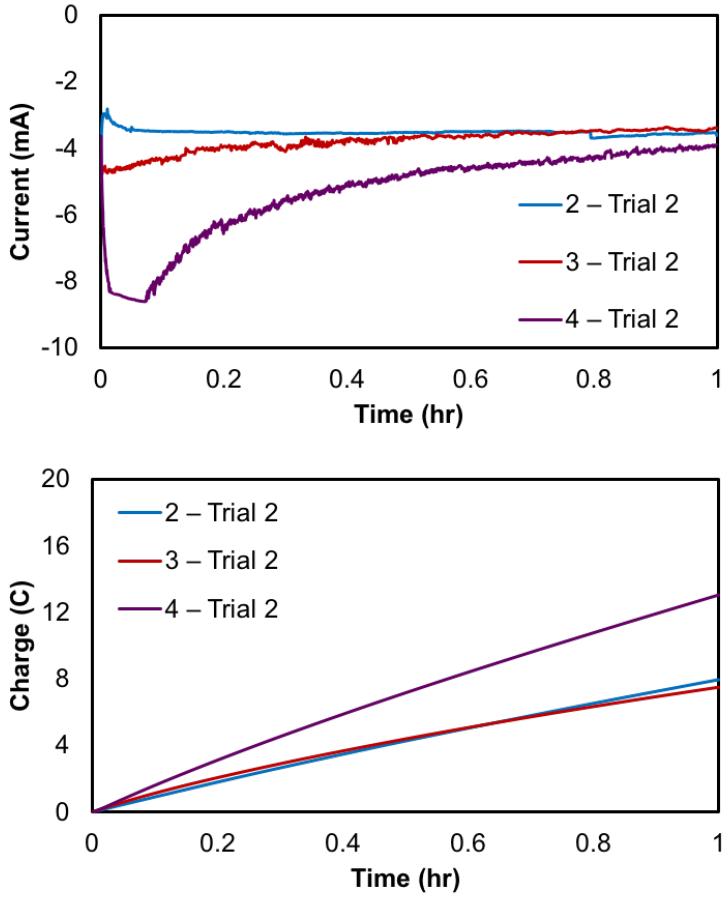

Figure S55. Replicate bulk electrolysis data for complex **2** – **4** measured at –2.75 V vs. $Fc^{+/0}$ over one hour. Electrochemical studies are performed in DMF solutions containing 0.1 M [nBu$_4$N][PF$_6$] under an atmosphere of CO_2 and in the presence of 2,2,2-trifluoroethanol (1.3 M) and catalyst (0.5 mM).

Table S11. Summary of the bulk electrolysis data from **Figures S12** and **S57.** The average error in a typical experiment for CO_2 and H_2 detection based on standard calibration curve is 10%.

Complex	*Charge (C)*	*FE CO (%)*	*FE H_2 (%)*
2 – Trial 1	7.95	15.3	12.7
2 – Trial 2	12.66	14.1	17.7
2 – Average	**10.31**	**14.7**	**15.2**
3 – Trial 1	7.47	88.4	<5
3 – Trial 2	13.61	82.0	<5
3 – Average	**10.54**	**85.2**	**<5**
4 – Trial 1	13.05	43.1	< 5
4 – Trial 2	19.07	46.9	< 5
4 – Average	**16.06**	**45.0**	**< 5**

Faradic Efficiency Corrected ($i_{cat}/i_p)^2$ Plots

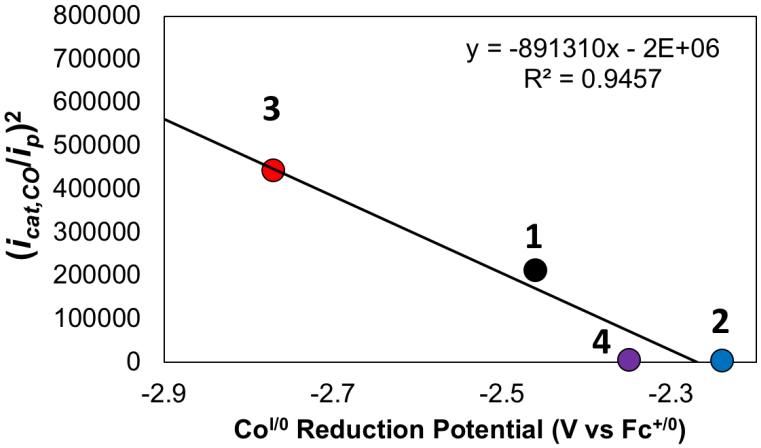

Figure S56. A plot of $(i_{cat,CO}/i_p)^2$ *vs*. the $Co^{I/0}$ reduction potential and its linear fit. The Faradic efficiency corrected current, $i_{cat,CO}$ was calculated by multiplying i_{cat} (measured in 1.5 M TFE under a CO_2 atmosphere) by the Faradic efficiency obtained from CPE experiments.

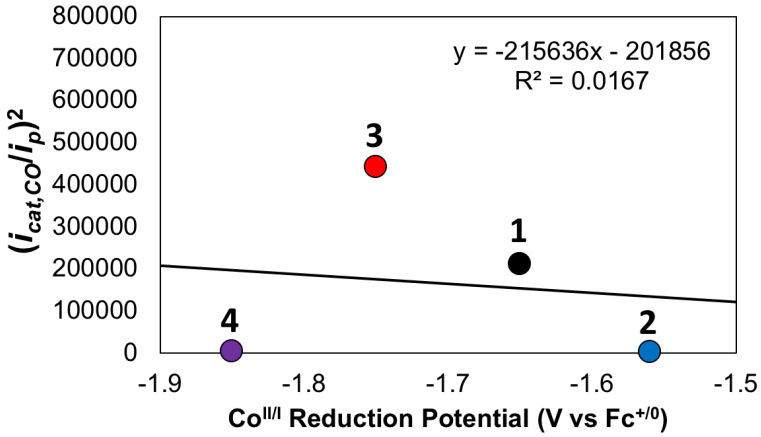

Figure S57. A plot of $(i_{cat,CO}/i_p)^2$ *vs*. the $Co^{II/I}$ reduction potential and its linear fit. The Faradic efficiency corrected current, $i_{cat,CO}$ was calculated by multiplying i_{cat} (measured in 1.5 M TFE under a CO_2 atmosphere) by the Faradic efficiency obtained from CPE experiments.

^{1}H NMR of Complex 4 with DCM

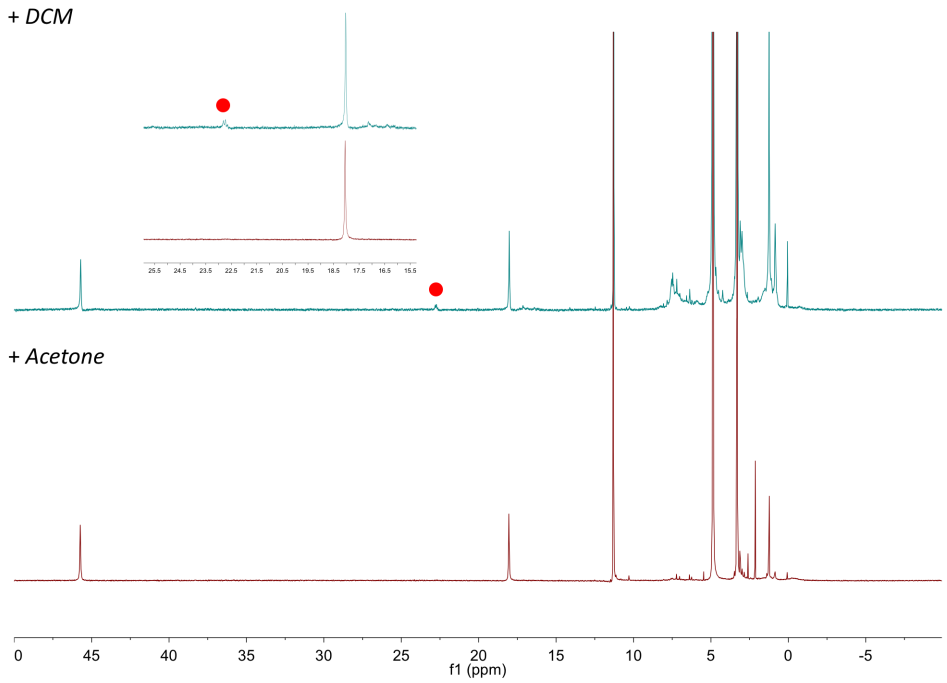

Figure S58. ^{1}H NMR spectra of complex **4** taken in MeOH-d_4 after exposure of the solid material to acetone (bottom), or DCM (followed by trituration with acetone) (top). The red circle indicates a new paramagnetic feature emerging in the presence of DCM.

TFE Titration of Complex 1

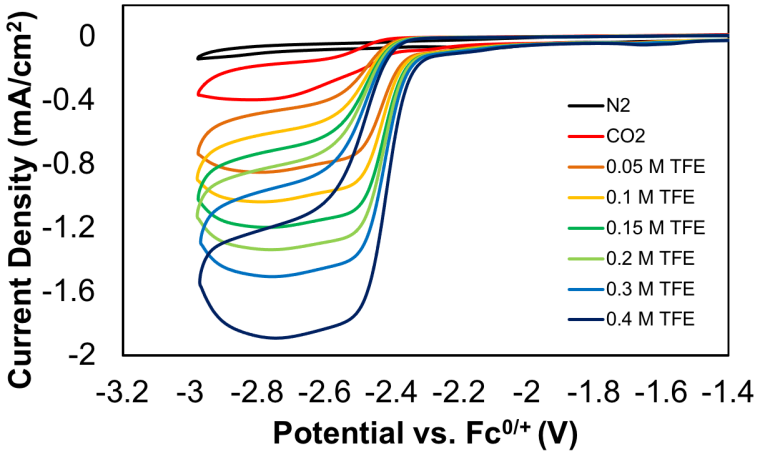

Figure S59. Cyclic voltammetry of complex **1** (0.1 mM) in a DMF solution containing 0.1 M [nBu$_4$N][PF$_6$] under CO_2 atmosphere with varying amounts of TFE. Scans were collected at 100 mV/s.

Table S12. Catalytic current for the titration of complex **1** (0.1 mM) with TFE. i_p = 0.007 mA/cm^2, extrapolated from the reversible Co$^{II/I}$ couple.

TFE (M)	i_{cat} (mA/cm^2)	i_{cat}/i_p
0	0.42	61.1
0.05	0.80	116.2
0.1	0.97	140.3
0.15	1.12	162.5
0.2	1.25	180.6
0.3	1.40	203.1
0.4	1.77	256.9

Calculation of Diffusion Coefficients for Complexes 2–4

Diffusion coefficients were calculated from the reversible Co$^{II/I}$ couple based on the Randles-Sevcik equation (below).

$$i_p = 0.4463 \times nFAC\sqrt{\frac{nFvD}{RT}}$$

i_p is the peak current, n the number of electrons transferred (n = 1 for the Co$^{II/I}$ couple), F is Faraday's constant (96,485 C/mol), A is the area of the electrode (0.07065 cm^2), C is the concentration of catalyst (5×10^{-7} mol/cm^3), n the scan rate (0.1 V/s), R is the gas law constant (8.314 J mol^{-1} K^{-1}), T is the absolute temperature (298.15 K) and D is the diffusion coefficient (cm^2/s). By plotting i_p as a function of $\nu^{1/2}$, the diffusion coefficient can be extrapolated.

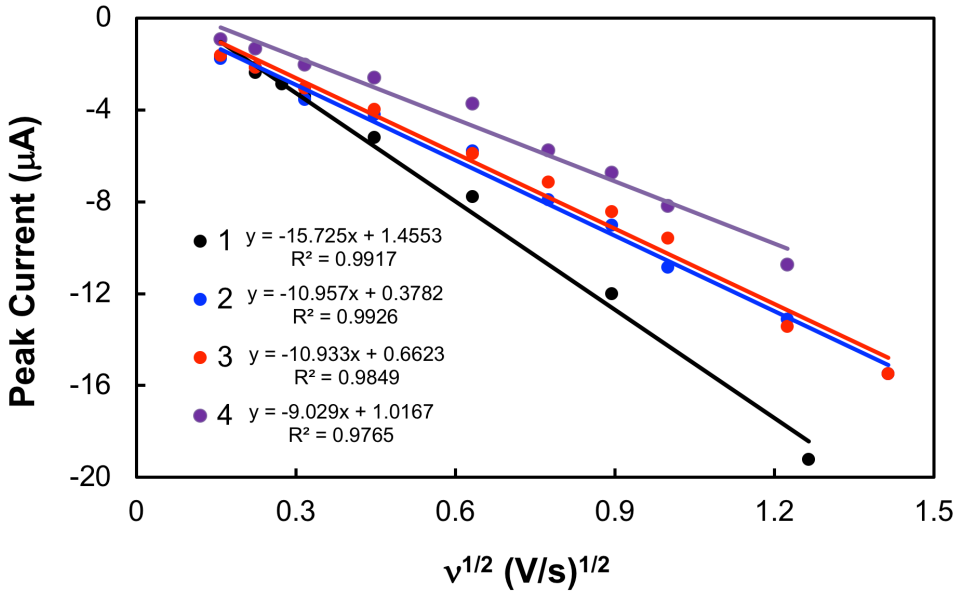

Figure S60. Linear fits of the peak current from the $Co^{II/I}$ couple as a function of the square-root of the scan rate for complex **1**–**4**. Diffusion coefficients for each complex was extrapolated from the slope and tabulated below.

Table S13. Tabulated diffusion constants measured for complexes **2–4** based on the VSR experiments found in **Figures S2**, **S4**, and **S6**.

Complex	Slope ($A \times s^{1/2} \times V^{-1/2}$)	D (cm^2/s)
1	-1.53×10^{-5}	2.73×10^{-6}
2	-1.10×10^{-6}	1.33×10^{-6}
3	-1.09×10^{-6}	1.33×10^{-6}
4	-9.03×10^{-7}	0.91×10^{-6}

Coordinates of Intermediates Examined in Density Functional Theory Studies

Listing S1. Coordinates of **$1^{(II)}$-CO_2**.

H	2.754712	0.001466	3.714494	C	2.388539	-0.53111	-5.30434
C	1.948436	0.343141	3.071947	H	3.272125	-0.25352	-5.87147
C	0.946962	1.179339	3.556688	C	2.33132	-0.28813	-3.92342
H	0.939415	1.486093	4.598725	H	5.583479	-0.78961	1.295062
C	-0.04181	1.617105	2.68514	C	5.16541	-0.56648	0.31771
H	-0.85204	2.254752	3.026693	C	3.778429	-0.53724	0.132325
C	0.003842	1.191297	1.348917	N	3.188969	-0.24478	-1.04284
N	0.977539	0.39882	0.854292	C	4.002482	0.035392	-2.08156
C	1.928551	-0.00819	1.717018	C	5.402217	0.060351	-1.98174
C	-1.66404	0.889015	-0.49799	H	6.007352	0.292377	-2.85316
C	-3.04576	1.08098	-0.65072	C	5.986531	-0.25052	-0.76096
H	-3.57308	1.779989	-0.00802	H	7.067071	-0.24553	-0.64938
C	-3.71777	0.337389	-1.61191	N	-0.89071	-1.56392	-2.99692
H	-4.78806	0.457179	-1.75376	H	-1.52717	-2.13004	-3.54473
C	-2.99657	-0.56182	-2.39224	N	3.438521	0.308332	-3.32525
H	-3.48048	-1.14187	-3.17276	H	4.121508	0.625156	-4.00011
C	-1.61528	-0.66422	-2.18987	N	2.954112	-0.8439	1.233238
N	-0.94338	0.040396	-1.25952	N	-1.01731	1.6126	0.500768
N	1.267856	-0.60732	-3.15696	H	-1.61718	2.304815	0.928616
C	0.232207	-1.21118	-3.7714	Co	1.139465	0.10811	-1.20273
C	0.212827	-1.51776	-5.13714	H	3.513474	-1.19205	2.002501
H	-0.66109	-1.98567	-5.58136	C	1.305331	2.102196	-1.69085
C	1.31067	-1.15978	-5.91407	O	2.1219	2.694236	-0.96769
H	1.323649	-1.36635	-6.98045	O	0.565107	2.412483	-2.63767

Listing S2. Coordinates of **$1^{(II)}$-CO_2H**.

H	2.752012	-0.2642	3.806903	H	3.407629	-0.0522	-5.6673
C	2.026413	0.184615	3.136553	C	2.494093	-0.12172	-3.71424
C	1.088954	1.104162	3.599393	H	5.66096	-1.0982	1.332681
H	1.056153	1.373982	4.65056	C	5.251421	-0.73127	0.397121
C	0.194158	1.667376	2.700483	C	3.869944	-0.63193	0.228527
H	-0.57131	2.364085	3.026805	N	3.29397	-0.17145	-0.90351
C	0.262327	1.283088	1.357003	C	4.114863	0.202074	-1.91058
N	1.189664	0.42101	0.882406	C	5.50994	0.17687	-1.80651
C	2.050243	-0.11674	1.774312	H	6.122277	0.490686	-2.64564
C	-1.35528	0.968802	-0.45175	C	6.080883	-0.30296	-0.63589
C	-2.74118	1.102199	-0.58673	H	7.160359	-0.34788	-0.52845
H	-3.27252	1.852223	-0.00981	N	-0.54618	-1.71063	-2.68463
C	-3.4135	0.23122	-1.43254	H	-1.13516	-2.38898	-3.15379
H	-4.49018	0.302379	-1.55279	N	3.527985	0.591664	-3.11148
C	-2.68932	-0.73628	-2.12385	H	4.187868	0.979736	-3.77433
H	-3.1775	-1.42213	-2.80847	N	3.01438	-1.00716	1.276639
C	-1.30397	-0.77562	-1.9618	N	-0.68005	1.77723	0.459578
N	-0.63105	0.060254	-1.14203	H	-1.25814	2.511832	0.848305
N	1.476286	-0.53507	-2.92722	Co	1.343512	0.103143	-1.06099
C	0.519014	-1.29752	-3.49975	H	3.519968	-1.46879	2.024076
C	0.541306	-1.66893	-4.84464	C	1.445001	2.088574	-1.59047
H	-0.26028	-2.27414	-5.25561	O	0.818261	2.635127	-2.48738
C	1.578542	-1.20277	-5.64716	O	2.323913	2.867081	-0.84296
H	1.613269	-1.45569	-6.70244	H	2.275662	3.780855	-1.20079
C	2.568643	-0.41175	-5.0807				

Listing S3. Coordinates of **$2^{(II)}$-CO_2**.

H	2.53163	0.018261	3.719313	N	3.198896	-0.02395	-1.08356
C	1.785032	0.426054	3.045449	C	4.033871	0.128107	-2.13641
C	0.746539	1.212098	3.52468	C	5.41497	-0.06179	-2.06702
C	0.658134	1.51894	4.996077	H	6.035139	0.073285	-2.94607
C	-0.18222	1.735509	2.619908	C	5.966683	-0.45532	-0.84437
H	-1.02957	2.320179	2.958302	C	7.444367	-0.7278	-0.73844
C	-0.01585	1.448201	1.265081	N	-0.93494	-1.19388	-3.19439
N	0.999027	0.704118	0.768418	H	-1.56935	-1.76514	-3.73691
C	1.882873	0.20839	1.664029	N	3.484258	0.509886	-3.36401
C	-1.65439	1.100608	-0.52688	H	4.200881	0.765765	-4.03181
C	-3.03972	1.080339	-0.46344	N	2.958278	-0.56127	1.218886
H	-3.56684	1.688141	0.26405	N	-0.949	1.949851	0.348338
C	-3.73625	0.229133	-1.34181	H	-1.56463	2.629842	0.778182
C	-5.23491	0.171433	-1.28597	Co	1.154055	0.469716	-1.31944
C	-3.01168	-0.54893	-2.22823	H	3.485884	-0.942	1.993782
H	-3.51382	-1.20023	-2.93556	C	1.418012	2.530235	-1.84292
C	-1.61086	-0.44315	-2.23749	O	2.242431	3.00835	-1.07988
N	-0.91564	0.352128	-1.38594	O	0.699304	2.774566	-2.79757
N	1.280897	-0.32518	-3.25348	F	-0.57255	1.949665	5.35641
C	0.251299	-0.95207	-3.87598	F	1.539225	2.486445	5.361908
C	0.311595	-1.38841	-5.211	F	0.944263	0.43044	5.754528
H	-0.55024	-1.86043	-5.67088	F	8.174571	0.152082	-1.46337
C	1.461628	-1.14541	-5.94122	F	7.753714	-1.96755	-1.20545
C	1.579875	-1.61967	-7.36392	F	7.886516	-0.67042	0.539251
C	2.541852	-0.50365	-5.319	F	2.34232	-0.78998	-8.11472
H	3.467626	-0.3193	-5.85194	F	0.374463	-1.72646	-7.97167
C	2.401092	-0.12674	-3.98555	F	2.160969	-2.8496	-7.43276
H	5.533568	-0.92302	1.212916	F	-5.75745	-0.67405	-2.20482
C	5.132087	-0.64318	0.245048	F	-5.79803	1.390172	-1.49408
C	3.757543	-0.39851	0.089047	F	-5.67364	-0.24573	-0.06677

Listing S4. Coordinates of **$2^{(II)}$-CO_2H**.

H	2.734002	-0.28255	3.745501	C	4.084788	0.207982	-1.96692
C	2.010138	0.168927	3.075701	C	5.480793	0.180271	-1.86563
C	1.076278	1.092775	3.542385	H	6.097932	0.491246	-2.7007
C	1.050506	1.438452	5.01817	C	6.045572	-0.30561	-0.69678
C	0.181712	1.666575	2.653575	C	7.549544	-0.3574	-0.51369
H	-0.57684	2.363374	2.991074	N	-0.58702	-1.67699	-2.74906
C	0.246729	1.286875	1.307497	H	-1.17777	-2.35829	-3.21242
N	1.166506	0.422497	0.826603	N	3.502789	0.600066	-3.16808
C	2.026759	-0.12571	1.714917	H	4.161507	0.993291	-3.82979
C	-1.37476	0.993323	-0.49835	N	2.982002	-1.02032	1.210046
C	-2.75732	1.136402	-0.63063	N	-0.69636	1.791382	0.418981
H	-3.28893	1.88191	-0.04874	H	-1.26592	2.532639	0.808893
C	-3.43257	0.274028	-1.48528	Co	1.316333	0.110418	-1.11466
C	-4.93676	0.399349	-1.6318	H	3.479563	-1.50265	1.950356
C	-2.71946	-0.69283	-2.18411	C	1.426955	2.090371	-1.63367
H	-3.21528	-1.36534	-2.87432	O	0.799666	2.635092	-2.5287
C	-1.33374	-0.74141	-2.01909	O	2.30858	2.85376	-0.88199
N	-0.65565	0.083831	-1.19501	H	2.27193	3.772757	-1.22766
N	1.444295	-0.51438	-2.98361	F	0.125987	2.375834	5.300824
C	0.482378	-1.27089	-3.55959	F	2.25267	1.903033	5.422411
C	0.504586	-1.64204	-4.90198	F	0.771223	0.342035	5.757922
H	-0.29747	-2.2409	-5.32022	F	8.206063	-0.09891	-1.66112
C	1.549961	-1.18097	-5.69927	F	7.938347	-1.57473	-0.07608
C	1.589665	-1.56448	-7.16567	F	7.947437	0.549575	0.405258
C	2.542196	-0.39449	-5.13577	F	2.620201	-0.98433	-7.80919
H	3.381184	-0.04194	-5.72418	F	0.448791	-1.20021	-7.78926
C	2.46344	-0.10528	-3.76841	F	1.715102	-2.90393	-7.30191
H	5.630825	-1.11203	1.267638	F	-5.42811	-0.47817	-2.52803
C	5.217297	-0.73912	0.336763	F	-5.27814	1.64134	-2.03363
C	3.838823	-0.63732	0.167158	F	-5.5519	0.172402	-0.44927
N	3.263392	-0.16792	-0.96316				

Listing S5. Coordinates of **$3^{(II)}$-CO_2**.

H	2.806205	-0.5819	3.645752	N	-1.05625	-0.67054	-3.12889
C	2.029284	-0.0641	3.097784	H	-1.76916	-1.16007	-3.65269
C	0.888214	0.446335	3.744808	N	3.323025	0.992459	-3.43496
C	-0.03759	1.138632	2.934361	H	3.984458	1.245062	-4.15774
H	-0.96203	1.530847	3.338551	N	3.322553	-0.37983	1.113208
C	0.203134	1.246216	1.565156	N	-0.71928	1.983402	0.797304
N	1.267019	0.725746	0.934714	H	-1.31279	2.547284	1.391835
C	2.168251	0.10683	1.717377	Co	1.202725	0.218395	-1.12325
C	-1.43226	1.525001	-0.31642	H	3.96182	-0.80034	1.774286
C	-2.76297	1.951627	-0.43619	N	0.689459	0.285456	5.098147
H	-3.18957	2.609694	0.316245	N	1.572251	-1.7325	-7.02613
C	-3.5282	1.483625	-1.4973	C	1.555229	-0.61568	5.846879
C	-2.93657	0.607769	-2.40426	H	2.596345	-0.27035	5.825131
H	-3.49109	0.220053	-3.25371	H	1.522256	-1.64404	5.45665
C	-1.59679	0.247241	-2.22295	H	1.234586	-0.63277	6.890047
N	-0.82004	0.709623	-1.20802	C	-0.57301	0.695697	5.695776
N	1.156258	0.092328	-3.23619	H	-0.7574	1.763245	5.525884
C	0.151716	-0.5897	-3.81293	H	-0.52445	0.53795	6.774869
C	0.234028	-1.20819	-5.06409	H	-1.42871	0.126948	5.299924
H	-0.6279	-1.74091	-5.44552	C	2.873955	-1.7484	-7.67845
C	1.430095	-1.11928	-5.80048	C	0.571887	-2.69961	-7.45961
C	2.472397	-0.36476	-5.21899	H	3.623036	-2.32214	-7.11033
H	3.443398	-0.28096	-5.68983	H	3.251044	-0.729	-7.8186
C	2.279241	0.208355	-3.96258	H	2.769727	-2.1989	-8.66728
H	5.862429	0.16213	1.045754	H	0.46409	-3.53141	-6.74753
C	5.359734	0.350289	0.10161	H	0.868641	-3.10888	-8.42703
C	3.981539	0.143124	-0.00581	H	-0.40763	-2.22277	-7.58759
N	3.264535	0.387333	-1.13577	C	1.032854	-1.8227	-0.79453
C	3.977872	0.799425	-2.21199	O	0.236136	-2.0759	0.119077
C	5.357424	1.047914	-2.184	O	1.752387	-2.46785	-1.56917
H	5.865366	1.379805	-3.08558	H	-4.56455	1.787495	-1.61244
C	6.061274	0.819942	-1.00731	H	7.131829	0.995341	-0.95596

Listing S6. Coordinates of **$3^{(II)}$-CO_2H**.

H	2.641557	-0.46311	3.754952	H	-1.4149	-2.00548	-3.49036
C	1.895029	0.001622	3.124052	N	3.285227	0.913488	-3.06348
C	0.892056	0.835913	3.667622	H	3.936927	1.340377	-3.71144
C	0.027819	1.454418	2.731571	N	3.009079	-0.96079	1.234958
H	-0.78599	2.09115	3.053323	N	-0.7048	1.811205	0.470185
C	0.176514	1.192796	1.377797	H	-1.27191	2.516384	0.925965
N	1.114267	0.368994	0.858213	Co	1.179781	-0.11417	-1.04508
C	1.969852	-0.18372	1.74951	H	3.533849	-1.45159	1.947658
C	-1.45901	1.049609	-0.43456	N	0.771182	1.040218	5.008055
C	-2.84828	1.185309	-0.46409	N	1.57952	-1.04416	-7.13832
H	-3.34254	1.878179	0.209376	C	1.611241	0.29316	5.941271
C	-3.57666	0.380914	-1.33682	H	2.672671	0.542945	5.815019
C	-2.89975	-0.50876	-2.15926	H	1.484181	-0.78949	5.812869
H	-3.42925	-1.13625	-2.86933	H	1.325489	0.549175	6.961523
C	-1.50154	-0.55379	-2.09431	C	-0.25569	1.938855	5.528499
N	-0.78074	0.200277	-1.23477	H	-0.17861	2.932213	5.070842
N	1.265751	-0.29408	-3.00046	H	-0.11436	2.056415	6.603091
C	0.316644	-0.97796	-3.6805	H	-1.26752	1.546012	5.35687
C	0.371418	-1.25012	-5.04103	C	2.675637	-0.46134	-7.90855
H	-0.45738	-1.77122	-5.50222	C	0.575785	-1.85637	-7.82116
C	1.46643	-0.78885	-5.80631	H	3.649038	-0.84209	-7.5726
C	2.437486	-0.03429	-5.10397	H	2.678609	0.633808	-7.83444
H	3.319888	0.344414	-5.60309	H	2.553632	-0.72665	-8.95876
C	2.296562	0.173241	-3.74014	H	0.425828	-2.81049	-7.30312
H	5.632731	-1.15794	1.115031	H	0.922708	-2.07638	-8.83107
C	5.182322	-0.72315	0.228454	H	-0.38956	-1.33616	-7.8954
C	3.792321	-0.57106	0.152581	C	1.087185	-2.13945	-0.73331
N	3.169152	-0.03864	-0.92173	O	0.124231	-2.56798	0.180804
C	3.942756	0.383699	-1.94358	O	1.783282	-2.99666	-1.2617
C	5.336687	0.306701	-1.93091	H	0.19356	-3.54694	0.226265
H	5.910055	0.652884	-2.78474	H	-4.65987	0.448921	-1.37328
C	5.960381	-0.26842	-0.82686	H	7.041774	-0.36177	-0.79272
N	-0.80837	-1.39184	-2.96152				

Listing S7. Coordinates of **4$^{(II)}$-CO$_2$**.

H	2.780407338	-0.507132393	3.805054234	H	-1.63174591	-1.631001663	-3.691784219
C	1.990773621	-0.068505397	3.208308962	N	3.399494554	0.648108033	-3.27981881
C	0.909140337	0.613679483	3.8042064	H	4.08768201	0.95606876	-3.954389671
C	-0.02807039	1.194413034	2.922916386	N	3.152623167	-0.815987401	1.246153469
H	-0.91330238	1.697316986	3.29099542	N	-0.79557551	1.670342439	0.707206405
C	0.148298118	1.052161492	1.545914009	H	-1.39507496	2.293590926	1.232775846
N	1.162187216	0.383330839	0.975169288	Co	1.199054011	-0.208492138	-1.07146865
C	2.069794237	-0.148370777	1.817632624	H	3.744033704	-1.252303396	1.941868639
C	-1.49588989	1.084715958	-0.352205129	F	8.154339112	0.581546344	-1.810530876
C	-2.85969445	1.375270271	-0.449621021	F	8.117879563	-0.629308917	0.010973606
H	-3.338546	2.003933437	0.293437683	F	7.828619471	1.521856349	0.130948312
C	-3.59983903	0.796553489	-1.480343144	F	-5.72834352	0.116685775	-2.274991179
C	-5.0550162	1.113206386	-1.648099742	F	-5.25310206	2.238927756	-2.395606826
C	-2.94445549	-0.040212058	-2.386241876	F	-5.67604416	1.334492278	-0.461367536
H	-3.47917192	-0.498937278	-3.210580147	N	0.781495155	0.715696356	5.167343714
C	-1.57647763	-0.261856637	-2.225787472	N	1.554204368	-1.386811753	-7.242176126
N	-0.83273602	0.286240738	-1.227743776	C	1.652112663	-0.066387974	6.036384291
N	1.239714014	-0.292336142	-3.179754909	H	2.70494131	0.202798515	5.888636667
C	0.226829388	-0.880420151	-3.841853829	H	1.540710864	-1.147267794	5.866106225
C	0.272118766	-1.255785765	-5.183920522	H	1.399757197	0.145622074	7.076535215
H	-0.6046614	-1.697322986	-5.640116352	C	-0.39600637	1.351665437	5.742182909
C	1.447205076	-1.013095774	-5.92821873	H	-0.51464506	2.37189988	5.358849727
C	2.498678351	-0.36204668	-5.250762198	H	-0.27223373	1.417946463	6.824429614
H	3.446738637	-0.169149113	-5.736389679	H	-1.31958522	0.79038794	5.533144628
C	2.347548859	-0.029536363	-3.901108455	C	2.761251747	-1.075546279	-7.995266954
H	5.733546813	-0.442976358	1.265802122	C	0.480826166	-2.138717349	-7.878877896
C	5.272505221	-0.212678761	0.310811892	H	3.641060512	-1.596767535	-7.591920252
C	3.901952564	-0.33494228	0.15443551	H	2.96508446	0.003405812	-7.992875231
N	3.227339955	-0.041177948	-1.001648757	H	2.626336863	-1.388571115	-9.031593599
C	4.006812804	0.364684467	-2.04578022	H	0.243172642	-3.050231899	-7.315008522
C	5.388675136	0.522861531	-1.973719626	H	0.797718227	-2.435707096	-8.879680099
H	5.946600518	0.833424312	-2.850726151	H	-0.43640949	-1.540477341	-7.976518406
C	6.049826884	0.227129771	-0.776729904	C	0.953322125	-2.280570276	-0.638510759
C	7.518282161	0.418342709	-0.622065179	O	0.06209264	-2.443705663	0.184289661
N	-0.95587061	-1.122836231	-3.136567509	O	1.744418851	-2.895901357	-1.34086352

Listing S8. Coordinates of **$4^{(II)}$-CO_2H**.

H	2.610901	-0.45517	3.759682	N	3.298379	0.901145	-3.0532
C	1.864969	0.00367	3.123806	H	3.951054	1.33069	-3.69847
C	0.858641	0.840611	3.659905	N	2.991486	-0.96412	1.244345
C	-0.00083	1.454369	2.715065	N	-0.72319	1.803859	0.449697
H	-0.81444	2.094964	3.029533	H	-1.28854	2.514008	0.900303
C	0.153163	1.184987	1.364544	Co	1.174042	-0.12365	-1.04798
N	1.091574	0.355756	0.852858	H	3.510816	-1.45519	1.961179
C	1.944501	-0.18868	1.751835	F	8.076147	0.228174	-1.74207
C	-1.47298	1.039881	-0.45343	F	7.838589	-1.67186	-0.69921
C	-2.86106	1.162198	-0.47811	F	7.930011	0.184234	0.43463
H	-3.36527	1.844816	0.197557	F	-5.64529	-0.43364	-2.23455
C	-3.58064	0.350694	-1.35457	F	-5.46939	1.696784	-1.8017
C	-5.08878	0.462754	-1.39461	F	-5.62478	0.266149	-0.16785
C	-2.90226	-0.53164	-2.17998	N	0.73214	1.052196	4.996479
H	-3.43056	-1.16057	-2.88737	N	1.608814	-1.03881	-7.13981
C	-1.50176	-0.56222	-2.11525	C	1.569853	0.312149	5.938882
N	-0.78755	0.199455	-1.25907	H	2.630466	0.568579	5.820803
N	1.276349	-0.30963	-2.99989	H	1.44919	-0.77101	5.811395
C	0.327504	-0.98386	-3.69093	H	1.273068	0.56794	6.955893
C	0.38745	-1.24912	-5.05104	C	-0.29353	1.958632	5.508722
H	-0.4415	-1.76326	-5.51963	H	-0.21332	2.947308	5.041977
C	1.489136	-0.78852	-5.8096	H	-0.15163	2.085709	6.582017
C	2.456801	-0.03799	-5.09729	H	-1.30548	1.5655	5.340706
H	3.340927	0.344598	-5.59025	C	2.712045	-0.45759	-7.90289
C	2.309838	0.161699	-3.73358	C	0.60891	-1.84932	-7.8324
H	5.620628	-1.12916	1.155121	H	3.681653	-0.84343	-7.56261
C	5.170106	-0.70689	0.26325	H	2.717414	0.637056	-7.82562
C	3.781659	-0.56605	0.172585	H	2.593934	-0.719	-8.95435
N	3.165622	-0.03353	-0.90764	H	0.453983	-2.80381	-7.31694
C	3.944572	0.383886	-1.92538	H	0.964449	-2.06889	-8.83926
C	5.340367	0.316122	-1.90278	H	-0.35404	-1.32653	-7.91426
H	5.922729	0.661181	-2.74892	C	1.078844	-2.1357	-0.74034
C	5.952316	-0.24642	-0.78853	O	0.105711	-2.55893	0.160067
C	7.458132	-0.37444	-0.70492	O	1.783253	-2.98739	-1.26333
N	-0.80719	-1.39485	-2.98134	H	0.170247	-3.53783	0.211231
H	-1.40827	-2.01211	-3.51256				

References

(1) Bruker Instrument Service V2011.4.0.0, Bruker AXS, Madison, WI. 2011.

(2) SAINT+ V8.27B, Bruker AXS Madison, WI. 2011.

(3) SADABS V2012-1, Bruker AXS Madison, WI, 2012.

(4) Bruker SHELXTL V2014/7, Bruker AXS Madison, WI. 2014.

(5) Sheldrick, G. M. A Short History of SHELX. *Acta Crystallogr. Sect. A Found. Crystallogr.* **2008**, *64*, 112–122.

(6) Sheldrick, G. M. Crystal Structure Refinement with SHELXL. *Acta Crystallogr. Sect. C Struct. Chem.* **2015**, *71*, 3–8.

(7) Hübschle, C. B.; Sheldrick, G. M.; Dittrich, B. ShelXle: A Qt Graphical User Interface for SHELXL. *J. Appl. Crystallogr.* **2011**, *44*, 1281–1284.

(8) Sampson, M. D.; Nguyen, A. D.; Grice, K. A.; Moore, C. E.; Rheingold, A. L.; Kubiak, C. P. Manganese Catalysts with Bulky Bipyridine Ligands for the Electrocatalytic Reduction of Carbon Dioxide: Eliminating Dimerization and Altering Catalysis. *J. Am. Chem. Soc.* **2014**, *136*, 5460–5471.

(9) Hansch, C.; Leo, a; Taft, R. W. A Survey of Hammett Substituent Constants and Resonance and Field Parameters. *Chem. Rev.* **1991**, *91*, 165–195.

(10) Huang, S. N.; Pascal, T. A.; Goddard, W. A.; Maiti, P. K.; Lin, S. T. Absolute Entropy and Energy of Carbon Dioxide Using the Two-Phase Thermodynamic Model. *J. Chem. Theory Comput.* **2011**, *7*, 1893–1901.

(11) Becke, A. D. Density-functional Thermochemistry. III. The Role of Exact Exchange. *J. Chem. Phys.* **1993**, *98*, 5648–5652.

(12) Lee, C.; Yang, W.; Parr, R. G. Development of the Colle-Salvetti Correlation-Energy Formula into a Functional of the Electron Density. *Phys. Rev. B* **1988**, *37*, 785–789.

(13) Stephens, P. J.; Devlin, F. J.; Chabalowski, C. F.; Frisch, M. J. Ab Initio Calculation of Vibrational Absorption and Circular Dichroism Spectra Using Density Functional Force Fields. *J. Phys. Chem.* **1994**, *98*, 11623–11627.

(14) Vosko, S. H.; Wilk, L.; Nusair, M. Accurate Spin-Dependent Electron Liquid Correlation Energies for Local Spin Density Calculations: A Critical Analysis. *Can. J. Phys.* **1980**, *58*, 1200–1211.

(15) Lebedev, V. I. Spherical Quadrature Formulas Exact to Orders 25–29. *Sib. Math. J.* **1977**, *18*, 99–107.

(16) Rassolov, V. A.; Ratner, M. A.; Pople, J. A.; Redfern, P. C.; Curtiss, L. A. 6-31G* Basis Set for Third-Row Atoms. *J. Comput. Chem.* **2001**, *22*, 976–984.

(17) Marenich, A. V; Cramer, C. J.; Truhlar, D. G. Universal Solvation Model Based on Solute Electron Density and on a Continuum Model of the Solvent Defined by the Bulk Dielectric Constant and Atomic Surface Tensions. *J. Phys. Chem. B* **2009**, *113*, 6378–

6396.

(18) Chapovetsky, A.; Welborn, M.; Luna, J. M.; Haiges, R.; Miller, T. F.; Marinescu, S. C. Pendant Hydrogen-Bond Donors in Cobalt Catalysts Independently Enhance CO 2 Reduction. *ACS Cent. Sci.* **2018**, *4*, 397–404.

(19) Cotton, F. A.; Wilkinson, G. *Advanced Inorganic Chemistry*, 4th ed.; Wiley: New York, 1980.